Texas A&M University
Mechanical Engineering Department
Turbomachinery Laboratory
Tribology Group

LEAKAGE AND ROTORDYNAMIC FORCE COEFFICIENTS IN AN (AIR IN OIL) *WET* SEAL: INFLUENCE OF SHAFT SPEED

TRC-SEAL-01-16
Research Progress Report to the Turbomachinery Research Consortium

by
Luis San Andrés
Mast-Childs Chair Professor
Principal Investigator

Xueliang Lu
Research Assistant

May 2016

***WET* (BUBBLY) SEALS FOR SUB-SEA MULTIPLE PHASE PUMPS AND *WET* COMPRESSORS**

TRC Project, TEES # 400124-00079

EXECUATIVE SUMMARY

As the oil and gas industry moves into deep sea, multiphase pumps and wet gas compressors become a preferred technology. The specific subsea environment determines both machine types have to handle oil and gas mixtures with changing gas volume fractions (GVF). A variation in mixture GVF affects system overall efficiency and reliability, including penalties in leakage and the rotordynamic performance of secondary flow components, namely seals. A better understanding of wet annular seal dynamic force characteristics will help to build robust subsea flow assurance systems.

The report describes measurements of leakage and force coefficients conducted in a short length (L/D = 0.36) smooth annular seal with clearance (c) = 0.203 mm (D=127mm), operating with an air in ISO VG 10 oil mixture. The test rig has a transparent seal cartridge supported by an elastic hollow pipe, and a spinning journal rigidly supported on two ball bearings. A sparger element installed upstream of the seal inlet mixes air and oil at a temperature (34 ºC) and continuously supplies air in oil mixtures with a steady GVF into the seal.

Measurement of seal leakage is conducted for operation with supply pressure (P_s) = 2.0, 2.5, 3.0, 3.5 bar (abs), discharge pressure (P_a) = 1 bar (abs), oil temperature (T_{in}) = 33 ~ 35 ºC, shaft speed (N) = 0, 1,500, 1,800, 2,500, 3,500 rpm (ΩR = 23.3 m/s), and a mixture with increasing GVF = 0 to 0.97. The seal operates under laminar flow for operations with either a pure oil or an air in oil mixture. The mixture mass flow rate ($\dot{m}_m$) decreases steady with an increase in inlet GVFs. The shaft speed has negligible influence on the test's shaft speed range 0 → 3,500 (ΩR = 23.3 m/s).

In dynamic load tests with frequency ($0 < \omega < 150$ Hz), the supply pressure (P_s) = 2.5 bar (abs), the discharge pressure (P_a) = 1 bar (abs), and the journal speed (N) = 0 rpm, 2500 rpm, 3500 rpm. With gas content, the seal direct stiffnesses (K_{XX} and K_{YY}) increase with whirl frequency (ω), and drop with GVF. Virtual mass (M) cannot be obtained from a curve fit of Re(H) as the dynamic stiffnesses are frequency dependent. The seal cross coupled stiffnesses (K_{XY} and K_{YX}) and direct damping (C_{XX} and C_{YY}) coefficient decrease continuously with an increase in inlet GVF. For tests shaft speed 2,500 rpm, the effective

damping coefficients C_{XXeff} and C_{XXeff} increase with whirl frequency over $0 < \omega < 110$ Hz. C_{XXeff} and C_{XXeff} decrease for $\omega > 110$ Hz. An increase in GVF drops the effective damping.

Even without shaft rotation or external periodic excitation, the air in oil mixture generates a dynamic pressure wave that excites the seal cartridge at a typical frequency ~ 20 Hz. This slow motion develops into a broad band frequency range for $0.6 < GVF < 0.9$. Likely, bubble clouds emit acoustic waves that oscillate at low normal modes induce this low frequency motion.

The current report does not include comparison of test data with prediction for force coefficients. Later, a detailed analysis will be conducted.

TABLE OF CONTENTS

LIST OF TABLES

LIST OF FIGURES

NOMENCLATURE

c	Seal radial clearance [m]
D	$D = 2R$, Journal diameter [m]
e	Amplitude of synchronous response of seal cartridge [m]
$F_{i(t)}$	External excitation force, $i = X, Y$ [N]
L	Seal length [mm]
$\dot{m}_m$	$\dot{m}_m = \dot{m}_g + \dot{m}_l$, Mass flow rate of air in oil mixture [kg/s]
$\overline{m}_m$	$\overline{m}_m = \dot{m}_g + \dot{m}_l$, Normalized mass flow rate air in oil mixture [-]
$\dot{m}_l$, $\dot{m}_g$	Mass flow rate for pure liquid and pure gas [kg/s]
N	Shaft rotational speed [rev/min]
P_a, P_s	Ambient pressure and supply pressure [Pa]
p_r	$p_r = P_s / P_a$, Pressure ratio [-]
Q_m	Volumetric flow rate for two-phase mixture [m^3/s]
Q_l , Q_g	Volumetric flow rate for pure liquid and pure gas [m^3/s]
R	Journal radius [m]
R_B	Bubble radius [m]
$\mathrm{Re_c}$	$\mathrm{Re_c} = \frac{\rho_m V_c c}{\mu_m}$, Circumferential flow Reynolds number [-]
$\mathrm{Re_z}$	$\mathrm{Re_z} = \frac{\rho_m V_z c}{\mu_m} = \frac{m_m}{\pi D \mu_m}$, Axial flow Reynolds number [-]
T	Temperature [K]
T_{in}	Seal inlet temperature [K]
V_c	$V_c = \frac{1}{2}\omega R$, Bulk flow circumferential velocity [m/s]
V_z	$V_z = Q/\pi Dc$, Bulk flow axial velocity [m/s]
X,Y	Seal cartridge displacements [m]
α	gas volume fraction [-]
β	liquid volume fraction [-]
ξ	Test rig structural damping ratio [-]
ΔP	$(P_s - P_a)$, Pressure difference [Pa]
λ	$\lambda = \dot{m}_g / \dot{m}_m$, gas mass fraction [-]
μ_l , μ_{ga}	Liquid and gas viscosity at ambient pressure and T = 34 ºC [Pa.s]
μ_m	Two-phase flow effective viscosity [Pa.s]
ρ_l, ρ_{ga}	Liquid and gas density at ambient pressure and T = 34 ºC [kg/m^3]
ρ_m	Mixture or two-phase fluid density [kg/m^3]
Ω	Shaft angular speed [rad/s]
ω	External load excitation frequency [Hz]
ω_n	System natural frequency [Hz]

Matrices

$\mathbf{C}$	System damping matrix, $\mathbf{C} = \mathbf{C_S} + \mathbf{C_{seal}}$ [N-s/m]
$\mathbf{C_S}$, $\mathbf{C_{seal}}$	Structure damping and seal damping matrices [N-s/m]
$\mathbf{F}$	External excitation force vector [N]
$\mathbf{H}$	$\mathbf{K} - \omega^2 \mathbf{M} + i\,\omega\,\mathbf{C}$. System complex stiffness matrix [N/m]
$\mathbf{K}$	System stiffness matrix, $\mathbf{K} = \mathbf{K_S} + \mathbf{K_{seal}}$ [N/m]
$\mathbf{K_S}$, $\mathbf{K_{seal}}$	Structure and seal stiffness matrices [N/m]
$\mathbf{M_S}$, $\mathbf{M_{seal}}$	Structure and seal mass matrices [kg]

$\mathbf{Z}$	Seal displacement vector relative to static journal [m]

Subscripts

S	Structure
a	Ambient
inlet	Inlet plane of seal (z = 0)
m	Mixture or two component flow
g	Gas
l	Liquid

Abbreviations

GVF	Gas volume fraction
LVF	Liquid volume fraction
SC	Seal cartridge
SFD	Squeeze film damper
SSV	Sub-synchronous vibration
WFR	Whirl frequency ratio

INTRODUCTION

A two phase flow condition could affect the leakage and dynamic force coefficients of annular seals restricting secondary flows in (*wet* gas) compressors and (multi-phase) pumps. A 2015 TRC report [1] details measurements conducted with a short length (L/D = 0.36) annular seal supplied with a gas-oil mixture and shows that an increase in the gas volume fraction (GVF) in an otherwise pure liquid drops the seal's leakage and reduces its damping coefficients. The loss in damping reduces the seal ability to dissipate mechanical energy, thus it is expected that there is an increase in amplitude of rotor synchronous response when traversing a critical speed. One other likely issue is that the rotating system may lose its stability.

As the oil and gas industry moves into deep sea, oil boosting and *wet* gas compression systems become a preferred technology as they add pressure to the unprocessed well effluent to increase the tieback distance from satellite wells thus eliminating a traditional separation facility. This new arrangement saves up to 30% of capital investment for an oil and gas separation station (the estimated cost of a multiphase pump is approximately 70% of a conventional separation equipment) [2].

One challenge for subsea flow assurance systems is that both compressors and pumps need to deal with gas in oil (two-phase) flows or even multiphase effluents (with gas volume fractions varying from 0 to 100%) that have dissimilar fluid characteristics, namely density (ρ) and viscosity (μ), as compared with the physical properties of a single phase component.

Research on the effect of GVF on the performance of *wet* annular seals began in 1993 when a pump annular seal was tested under operation of an air in water mixture [3]. The interest of static and dynamic characteristics on *wet* annular seals started to grow in 2005 when a single stage compressor tested at the K-lab in Norway operated with a mixture of natural gas and a hydrocarbon liquid [4]. A 0.5Xrev subsynchronous vibration (SSV) occurred when the liquid content increased. The authors suspect that the liquid could have been entrained in the seals and caused the subsynchrounous rotor motion.

Since 2014, the Turbomachinery Research Consortium (TRC) funds a project to experimentally investigate the effect of air in oil mixture on annular seal leakage and dynamic force coefficients. A prior TRC report [1] shows that in tests conducted with a

wet seal (L/D = 0.36) at a pressure supply/pressure discharge ratio = 3.0 and 3.5 and with a non-rotating journal, the flow rate for an air in ISO VG 10 oil mixture increases from the pure gas condition, to that of the mixture with increasing GVF, and to the pure liquid condition. The w*et* seal stiffness, mass and damping force coefficients are determined for a seal operating with a pressure supply/pressure discharge ratio = 2.0 and supplied (a) with air (only) and (b) an oil in air mixture with inlet LVF = 2% and 4%. The experimental results, first of its kind, reveal a small amount of liquid increases ten-fold (or more) the damping coefficients of the *wet* seal [1]. Predictions from a computational bulk-flow model also demonstrate that the seal damping coefficients vary greatly with small contents of liquid in the oil/gas mixture. The agreement of prediction with the test force coefficients is not compelling on account of the likely inhomogeneity of the mixture flowing through the seal[1].

The work in 2015-2016 presents further experimental results and predictions for the leakage and rotordynamic behavior of a short length (L/D = 0.36) smooth surface annular seal. The operation conditions include (a) seal inlet GVF = 0, 0.2, 0.4, 0.6, 0.8, 0.9; (b) shaft speed (N) = 0, 2,500, 3,500 rpm; (c) supply pressure/discharge pressure = 2.5, and (d) a dynamic load with excitation frequency (ω) = 30 Hz to 150 Hz, in steps of 10 Hz.

The report also discloses finding an unusual low frequency vibration of the test element. As gas is injected into the flowing liquid, the air in oil mixture generates a dynamic pressure that excites the seal cartridge with a typical broad band frequency of less than 20 Hz. The amplitude of the low frequency band motion varies with the magnitude of the inlet GVF.

[1] Material reproduced from San Andrés, L., Lu, X., Liu, Q., 2016, "Measurements of Flow Rate and Force Coefficients in a Short-Length Annular Seal Supplied with a Liquid/Gas Mixture (Stationary Journal)," Tribol. Trans., Paper accepted: Sep 28th, 2015. Copyright 2015 by Society of Tribologists and Lubrication Engineers.

BRIEF LITERATURE REVIEW

A multiphase pump at times needs to handle a gas-oil two-component flow with up to 100% of gas [2] and a *wet* gas compressor may need to work with up to 5% liquid volume fraction [5, 6]. Operation with a high surface speed and with a large pressure difference makes seals (long ones as in balance pistons) to produce large dynamic reaction forces that affect the rotordynamics of a turbomachine [1]. A variation in liquid volume fraction (LVF) does affect the force coefficients of an annular seal. Vannini, et al. (2016) [7] conclude that a tooth on stator labyrinth seal is not a good option for a balance piston in a *wet* gas compressor. The liquid is likely to accumulate in the seal cavities even at a very low LVF. Although the exact mechanism by which the liquid interacts with the rotor is not captured, the authors believe that the entrapped liquid is the source of a 0.5X subsynchronous vibration in the *wet* gas compressor.

Beatty and Hughes (1987) [8] model a two-phase turbulent flow in an annular seal assuming an adiabatic flow and a homogeneous mixture. The results show that the leakage for a pure liquid flow is much higher than that of a two-phase flow. The same authors (1990) [9] extend to a stratified flow model to estimate the seal leakage under operation with a high shaft rotational speed where the liquid phase and gas phase travels through the seal clearance as two separate layers due to strong centrifugal fluid inertia effects. The prediction shows that the leakage estimated from the stratified flow model is close in magnitude to that from the homogeneous-equilibrium model for an identical seal geometry and operation conditions. The authors conclude that the insensitivity of leakage on the degree of flow inhomogeneity is encouraging as it implies that the estimation of flow rate requires no precise information about the actual flow pattern or interfacial shear stresses.

Iwatsubo and Nishino (1993) [3] investigate experimentally the static and dynamic force coefficients of a pump annular seal (with diameter D =70 mm, length L = 70 mm, and radial clearance c = 0.5 mm) operating with an air-water mixture whose gas volume fraction (GVF) ranges from 0 (no gas) to 0.70. The operating shaft speed is up to 3,500 rpm (ΩR = 13 m/s). The tests show a steady decrease of both the radial and tangential reaction fluid film forces with the increase in GVF due to the gas compressibility. In addition, the authors report of a random vibration due to the two-phase flow, that becomes

very large in magnitude at GVF = 0.7. However, the authors do not offer the frequency component of the noise.

San Andrés (2012) [10] develops a modified bulk-flow model to predict the leakage rate, power loss, and dynamic force coefficients of textured annular seals operating with a homogeneous gas-liquid mixture. Predictions show the seal leakage, direct damping and power loss decrease steadily with an increase in GVF at the seal inlet. The seal force coefficients also decrease rapidly with excitation frequency if the mixture has a larger GVF.

San Andrés, Lu and Liu (2015) [1] conduct experiments on a smooth annular seal (L/D = 0.36) supplied with an ISO VG 10 air in oil mixture. Tests with a non-rotating journal and at a pressure supply/discharge ratio = 3.0 and 3.5 show the seal mass flow rate decreases steadily with an increase in GVF. Predictions of seal leakage match well with the experimental results, all conducted under laminar flow conditions. Dynamic load tests with a supply pressure (P_s) = 2.0 show that with a small volume fraction of oil in gas (2%) compared with that of a pure gas condition, the seal direct damping will increase 10 times.

This report (2015 – 2016) delivers further test results for a short length annular (L/D = 0.36) seal operating with an air in oil mixture and under a spinning shaft. The circumferential and axial flow Reynolds number shows the seal operates in a laminar flow condition.

TEST RIG DESCRIPTION

Figure 1 shows the *wet* seal test rig and auxiliary systems. The rig consists of (i) an air-oil circulation system, (ii) a mechanical structure system containing the test seal, and (iii) a control and data acquisition system.

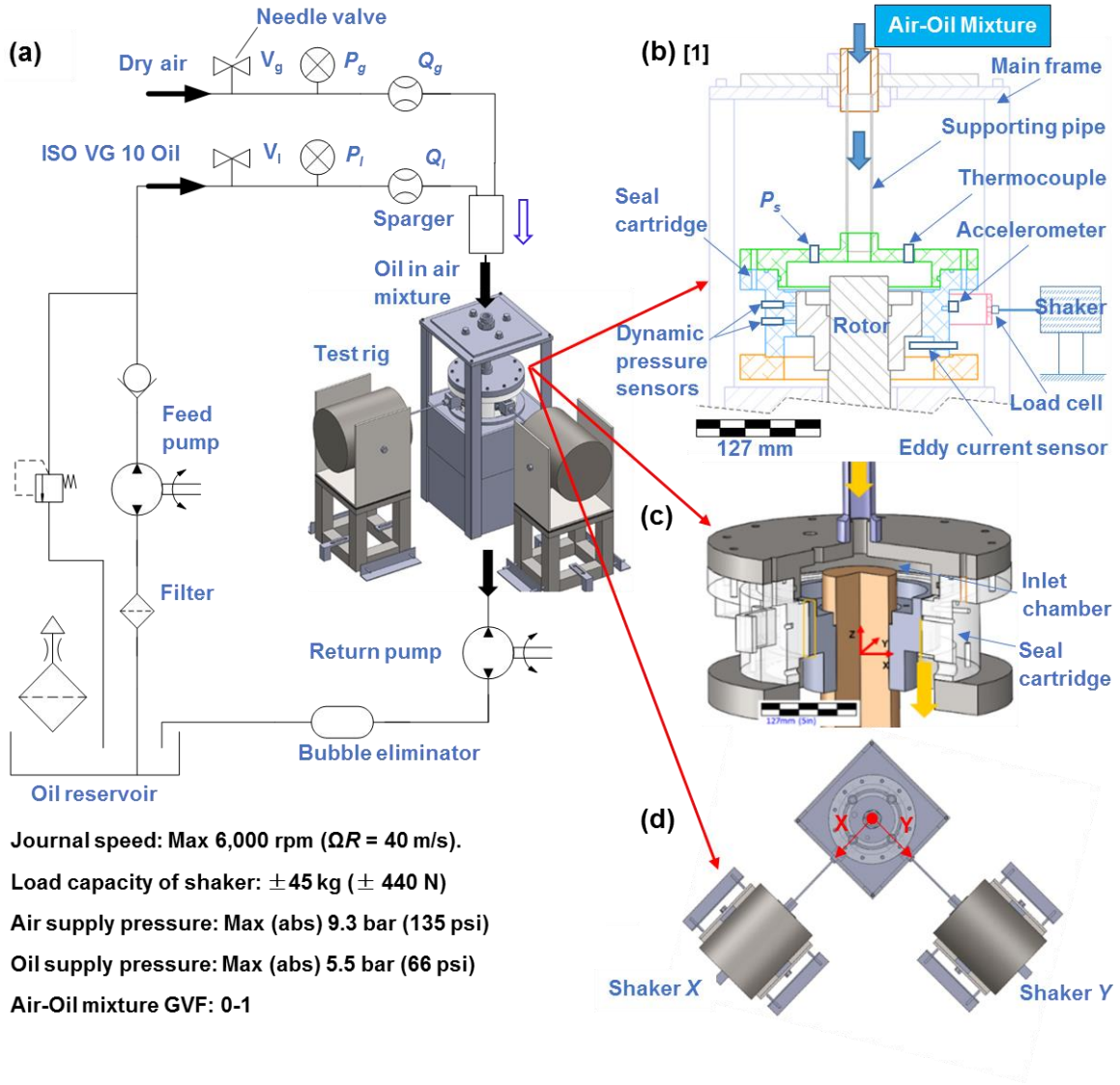

Figure 1. Schematic view (a) w*et* seal air-oil loop circulation system, (b) cross section of test rig mechanical system and instrumentation, (c) cut view of seal-rotor assembly, (d) top view of test rig with shakers.

The air and oil flow circulation system consists of a gear pump and oil supply line that continuously delivers ISO VG 10 oil at a constant volumetric flow rate, and an air supply line that draws dry air from a large pressurized tank into a sparger element to make an air in oil mixture. This mixture flows through a supply pipe into a plenum atop the seal

cartridge, and through the seal annular gap with clearance (c), to finally exit into a plenum. Here, the mixture remains for ~ three minutes, until most of the bubbles release their air content into the atmosphere. A second pump returns the accumulated lubricant, first passing through a bubble eliminator installed in the return line. The oil then flows back into an oil reservoir for recirculation. During the tests, two needle valves adjust the oil flow rate (Q_l) and air volumetric flow rate (Q_g). Both the oil and the compressed (dry) air mix at a uniform temperature [2] of ~34 ºC. At this temperature, the oil viscosity (μ_l) is ~10.6 cP and its density (ρ_l) is 830 kg/m^3.

The test rig mechanical system. Figure 1(b) depicts a cross section of the *wet* seal test rig mechanical system composed of a seal cartridge (SC), a rigid rotor assembly, and a hollow pipe that support the seal cartridge (SC) atop. Two orthogonally mounted electromagnetic shakers, via two long stingers, excite the seal cartridge at a maximum load of 440 N (100 lbf). Figure 1(c) shows a cut view of the seal and journal assembly. The inlet chamber in the seal cartridge (SC) allows air and oil to mix more uniformly prior to entering the seal clearance (c). And the seal cartridge made of transparent acrylic plastic permits eye-viewing of the air-oil mixture.

Table 1 lists the seal dimensions and the oil and air physical properties. The smooth surface annular seal has a diameter (D) of 127 mm, an axial length (L) equal to 46 mm, and a "cold" radial clearance (c) of 0.127 mm at 18 ºC. The seal clearance is a function of the temperature of the seal cartridge and also the mixture. The dissimilar thermal expansion coefficients of the steel rotor and the acrylic cartridge determine the seal clearance during operation. Appendix A shows the predicted and measured seal clearance for increasing operating temperature. The seal "hot" radial clearance (c) at T = 34 ºC is ~ 0.203 mm.

An electric DC motor, drives through a pulley mechanism (with a gear ratio of 1.8), the rotor that is supported by two stiff ball bearings. The maximum spinning speed of the rotor is 6,000 rpm. The top surface speed of the journal is ΩR = 40 m/s, where Ω is the shaft angular speed, and R = 63.5 mm is the shaft radius.

[2] The operating temperature is higher than room temperature (~20 ºC) because the mixture warms due to shear drag from the rotating journal.

Table 1. Annular seal dimensions and fluids properties.
ρ_l/ρ_{ga} = 691, μ_l/μ_{ga} = 530

Seal Diameter	$D = 2R$	127 mm
Length	L	46 mm
Radial Clearance	c	0.203 ± 0.005 mm (at 34 ºC)
Lubricant Parameters		
ISO VG10 Absolute Viscosity	μ_l	10.6 cP (34 ºC)
Density	ρ_l	830 kg/m^3
Air Viscosity	μ_{ga}	0.02 cP (34 ºC)
Density	ρ_{ga}	1.2 kg/m^3 at P_a = 1 bar (abs)

The control and data acquisition system sets the shaft speed through manually adjusting the armature supply voltage (V) and current (I) of the DC motor. A LabVIEW® code and a power amplifier control the magnitude and frequency of the external load exerted by two electromagnetic shakers on the seal cartridge.

Two piezoelectric load cells attached to the seal housing measure the excitation forces. Two eddy current sensors and two piezoelectric accelerometers record the ensuing test seal motions and accelerations along two orthogonal directions (X & Y). During testing, an oscilloscope displays the cartridge motion detected by the two eddy current sensors. An I/O-Tech® 652U box acquires voltage signals from sensors at a rate of 12,800 samples/s. A computer collects and stores data. The acquisition time lasts typically 10.24 s.

FLOW RATE THROUGH SEAL

2015 TRC report [1] details the procedure to measure the flow through the seal with a mixture delivered at a known supply pressure (P_s). First, the feed pump is turned on and valve V_l is open to pressurize the oil supply line. Next, the needle valve V_g (see Figure 1 (a)) is open to inject air into the sparger element to generate the air in oil mixture with an inlet GVF flowing through the seal.

An oil turbine flow meter and an air mass flow meter installed well upstream of the sparger element record the oil flow rate (Q_l) and air volumetric flow rate (Q_g) at supply pressure (P_s). These three recorded parameters (Q_l, Q_g and P_s) determine the mixture gas volume fraction at the seal inlet GVF (α_{inlet}) as

$$\alpha_{inlet} = \frac{Q_g (P_a / P_s)}{Q_l + Q_g (P_a / P_s)} \tag{1}$$

The mass flow rate of the liquid ($\dot{m}_l = \rho_l \times Q_l$) adds to that of the gas ($\dot{m}_g = \rho_{ga} \times Q_g$) to make the mixture mass flow rate through the seal, $\dot{m}_m = \dot{m}_l + \dot{m}_g$ [1]. Note the gas flow meter measures the air volumetric flow rate at a standard condition (20 ^{o}C and 1 bar (abs)).

Once an air in oil mixture fills the plenum in the top of the seal cartridge and flows through the seal clearance (c), the DC motor is turned on to spin the shaft at a preset speed, i.e., 2,500 rpm (ΩR = 16.6 m/s). As the operation with a mixture progresses for about 10 minutes, the operator witnesses a steady increase of the oil leakage (Q_l) and oil temperature (in the oil reservoir) while the supply pressure (P_s) remains constant. The increase of oil temperature arises from the heat generated by (i) the rotational shear drag when flowing through the small clearance (c) and (ii) work done by the supply and return gear pumps.

Thus, the temperature of the acrylic seal cartridge (SC) increases accordingly due to the heat transmitted from the mixture. The material of the SC has a larger thermal expansion coefficient than that of the steel journal. As the SC[3] expands more than the journal, the seal clearance (c) increases accordingly. The enlarged clearance allows more mixture to flow through the seal.

During an experiment, the mixture mass flow rate at various inlet GVF follows a sequence: α_{inlet} = 0 (pure oil) → α_{inlet} = 0.2 → α_{inlet} = 0.4 → α_{inlet} = 0.6 → α_{inlet} = 0.8 → α_{inlet} = 0.92 → α_{inlet} = 0.97 (for P_s = 2.0 bar (abs) only). Therefore, even in tests conducted in a pure gas condition, the seal clearance still remains ~ 0.203 mm (at 34 ^{o}C), because the SC is already "warmed up" when operating with a mixture. Appendix A elaborates on the measurement and prediction of the operating seal clearance.

The seal mass flow rate for a pure liquid flowing through the seal under laminar flow condition is

$$\dot{m}_l = \rho_l Q_l = \rho_l \left(\frac{c^3}{12\mu_l} \frac{\Delta P_z}{L} \right) \pi D \tag{2}$$

During the experiment, the oil temperature in the oil reservoir reaches an equilibrium point at ~34 ^{o}C (fluctuates from 33-35^{o}C). The oil viscosity (μ_l) and seal clearance (c) used for prediction of seal leakage and force coefficients is at 34 ^{o}C. Note the clearance (c) dominates the change in leakage as $Q_l \sim c^3$.

[3] Note the outside diameter of SC is not constrained.

Figure 2 shows photographs of the air in oil mixture flowing through the seal while the shaft spins at (N) = 1,800 rpm (30 Hz, ΩR = 12 m/s). The supply pressure (P_s) = 2.0 bar (abs), and the inlet gas volume fraction (GVF) = 0.9. The gas mass fraction (λ) = 6.2% is constant along the seal length. The photographs (a), (b) and (c) are three consecutive frames of a video recorded at 60 frames/s and with a stroboscope whose light refresh rate coincides with the shaft rotational speed. The photographs span an angle $\theta \sim 30^o$.

With an air in oil mixture and a spinning shaft, there are no visible single gas bubbles in the mixture. Instead, the bubbles coalesce and liquid merges into drops. The shaft surface speed shears the liquid to make streamlets, as shown in graph (c). Note at α_{inlet} = 0.9, the gas volumetric flow rate at the seal inlet is Q_g = 41.5 SLPM while the oil volumetric flow rate is Q_l = 0.42 LPM.

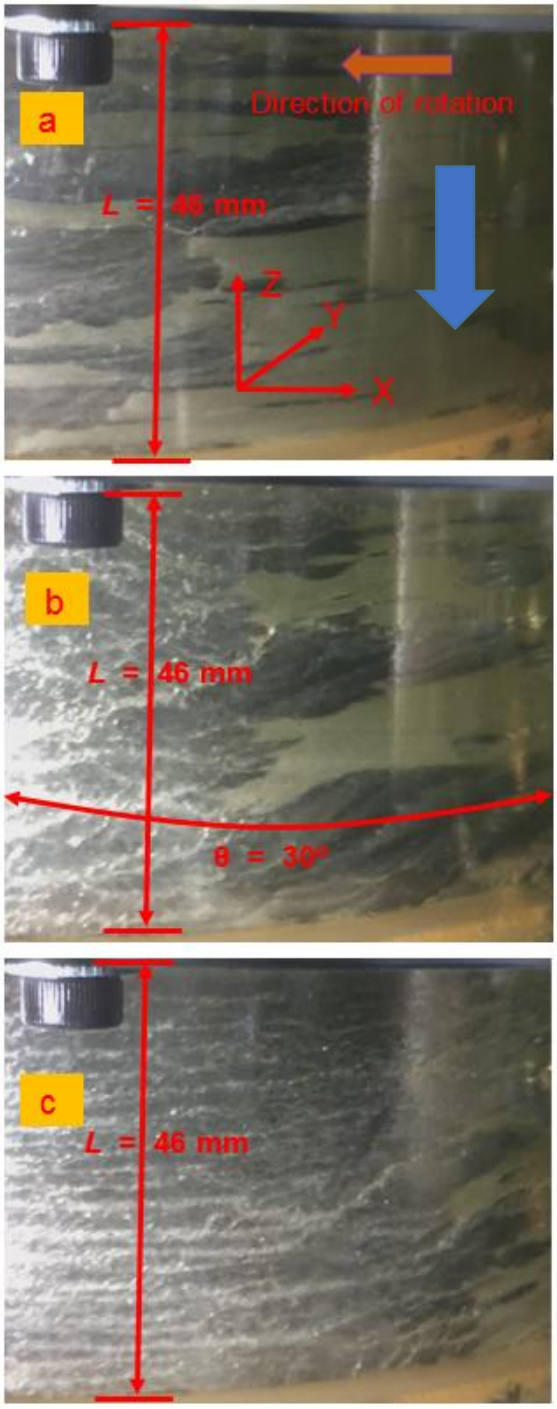

Figure 2. Flow visualization of *wet* seal operating with a gas and oil mixture. Inlet GVF = 0.9, journal speed (N) = 1800 rpm (30 Hz). Pictures taken with a stroboscope light at 30 Hz. Seal inlet pressure (P_s) = 2.0 bar (abs), discharge pressure (P_a) = 1 bar (abs). Inlet temperature (T_{in}) = 33 ºC~35 ºC.

Table 2 shows the seal leakage ($\dot{m}_l$) for a pure oil condition. The operating conditions are supply pressure (P_s) = 2.0, 2.5, 3.0, 3.5 bar (abs); and shaft speed (N) = 0, 1,500, 1,800, 2,500, 3,500 rpm. The tests for (P_s) = 2.0, 3.0, 3.5 bar (abs) are conducted on different days, therefore, the operating temperature varies from 25 - 34 ^{o}C. The leakage for a pure oil ($\dot{m}_l$) serve as a reference to normalize the mixture leakage ($\dot{m}_m$) at the same operating condition.

Table 2. Seal leakage for a pure oil ($\dot{m}_l$) condition. Supply pressure (P_s) = 2.0, 2.5, 3.0, 3.5 bar (abs), discharge pressure (P_a) = 1 bar (abs), shaft speed (N) = 0, 1,500, 1,800, 2,500, 3,500 rpm (ΩR = 23.3 m/s).

supply pressure, P_s (bar (abs))	shaft speed, N (rpm)	Measured oil leakage, $\dot{m}_l$ (g/s)	Predicted oil leakage, $\dot{m}_l$ (g/s)	Clearance c (mm)	Temperature T (^{o}C)	Oil viscosity, μ (cP)
2.0	1,800	39.5 ± 1.0	39.7	0.198	32	11.8
2.5	0	68.5 ± 0.7	70.2	0.203	34	10.6
2.5	1,500	67.8 ± 0.7	70.2	0.203	34	10.6
2.5	2,500	66.7 ± 1.7	70.2	0.203	34	10.6
2.5	3,500	68.0 ± 1.2	70.2	0.203	34	10.6
3.0	0	46.2 ± 0.9	43.3	0.172	27	14.1
3.5	0	44.5 ± 1.1	44.3	0.165	25	15.2

With a pure oil and operation at a shaft speed of 3,500 rpm (ΩR = 23.3 m/s), a supply pressure of 2.5 bar (abs), and an inlet temperature of 34 ^{o}C, the circumferential flow Reynolds number $\mathrm{Re}_c = \frac{\rho_l V_c c}{\mu_l}$ = 363 and the axial flow Reynolds number $\mathrm{Re}_z = \frac{\rho_l V_z c}{\mu_l} = \frac{\dot{m}_l}{\pi D \mu_l}$ = 16. Thus the flow is laminar[4].

The test results show a constant seal leakage at a fixed supply pressure (P_s) = 2.5 bar (abs) while the shaft speed increases from 0 rpm to 3,500 rpm. Hence, shaft speed (N) has a minor influence on the oil mass flow rate ($\dot{m}_l$) over the test speed range.

The mixture leakage is normalized as $\overline{m}_m = (\dot{m}_m / \dot{m}_l)$. That is, at a certain supply pressure (P_s), a shaft speed (N), and an inlet GVF, $\overline{m}_m$ is the ratio of the mass flow rate of the air in oil mixture ($\dot{m}_m$) to the mass flow rate for a pure oil ($\dot{m}_l$). As there is no phase change between the oil and the air, the gas mass fraction ($\lambda = \dot{m}_g / \dot{m}_m$) is invariant along the seal length. In addition, the gas volume fraction (GVF) in the downstream of the seal is larger than that at the upstream of the seal due to the expansion in air volume caused by

[4] Under this condition, the average circumferential flow velocity V_c = ½ ΩR = 11.7 m/s, and the average axial flow velocity, $V_Z = Q_l/(\pi Dc)$ = 0.95 m/s.

the drop in local pressure. The gas volume fraction at the seal exit equals $\alpha_{outlet} = \alpha_{inlet} \times P_s/P_a$.

Figure 3(a) shows as symbols the normalized seal leakage ($\overline{m}_m = \dot{m}_m / \dot{m}_l$) versus gas volume fraction at the seal inlet (α_{inlet}). The operating conditions for the experiments are the same as those with a pure oil, except that the lubricant is an air in oil mixture with α_{inlet} = 0 to 0.97. Figure 3(b) shows a zoom of the normalized seal leakage ($\overline{m}_m$) at a typical regime of $0.8 < \alpha_{inlet} < 0.97$. In the graph, the line stands for predicted results based on the model advanced by San Andrés [10].

In Figure 3(a), at a specific shaft speed (N) and inlet pressure (P_s), say, 1,800 rpm and 2.0 bar (abs), the flow rate drops steadily as the inlet GVF increases. Similar to the test results shown in Ref. [1], the seal leakage drops quickly as the inlet GVF > 0.9 due to the reduction in mixture density (ρ_m) with gas content.

For an air in oil mixture with inlet GVF = 0.92, at operation shaft speed of 3,500 rpm (ΩR = 23.3 m/s), supply pressure of 2.5 bar (abs), and inlet temperature of 34 ^{o}C, the exit circumferential flow Reynolds number $\mathrm{Re}_c = \frac{\rho_m V_c c}{\mu_m}$ = 298, and the exit axial flow Reynolds number $\mathrm{Re}_z = \frac{\rho_m V_z c}{\mu_m} = \frac{\dot{m}_m}{\pi D \mu_m}$ = 307, evidencing that the flow is still laminar.

At supply pressure (P_s) = 2.5 bar (abs) and inlet GVF = 0.4, the mixture mass flow rate ($\overline{m}_m$) in Figure 3(a) varies little as the shaft speed (N) increases from 0 rpm to 3,500 rpm (ΩR = 23.3 m/s). Therefore, shaft speed (N) has little influence on the flow rate.

As shown in Figure 3(a), predictions of seal leakage ($\dot{m}_m$) match well with test data over the range of $0 < \alpha_{inlet} < 0.9$. At $0.9 < \alpha_{inlet} < 0.97$ both the experimental mass flow and the predicted flow rate show a sudden drop. However, within this range ($0.9 < \alpha_{inlet} < 0.97$) the prediction is slightly higher than the measured leakage, as shown in zoom of Figure 3(b). The discrepancy is attributed to the inhomogeneous characteristic of the mixture.

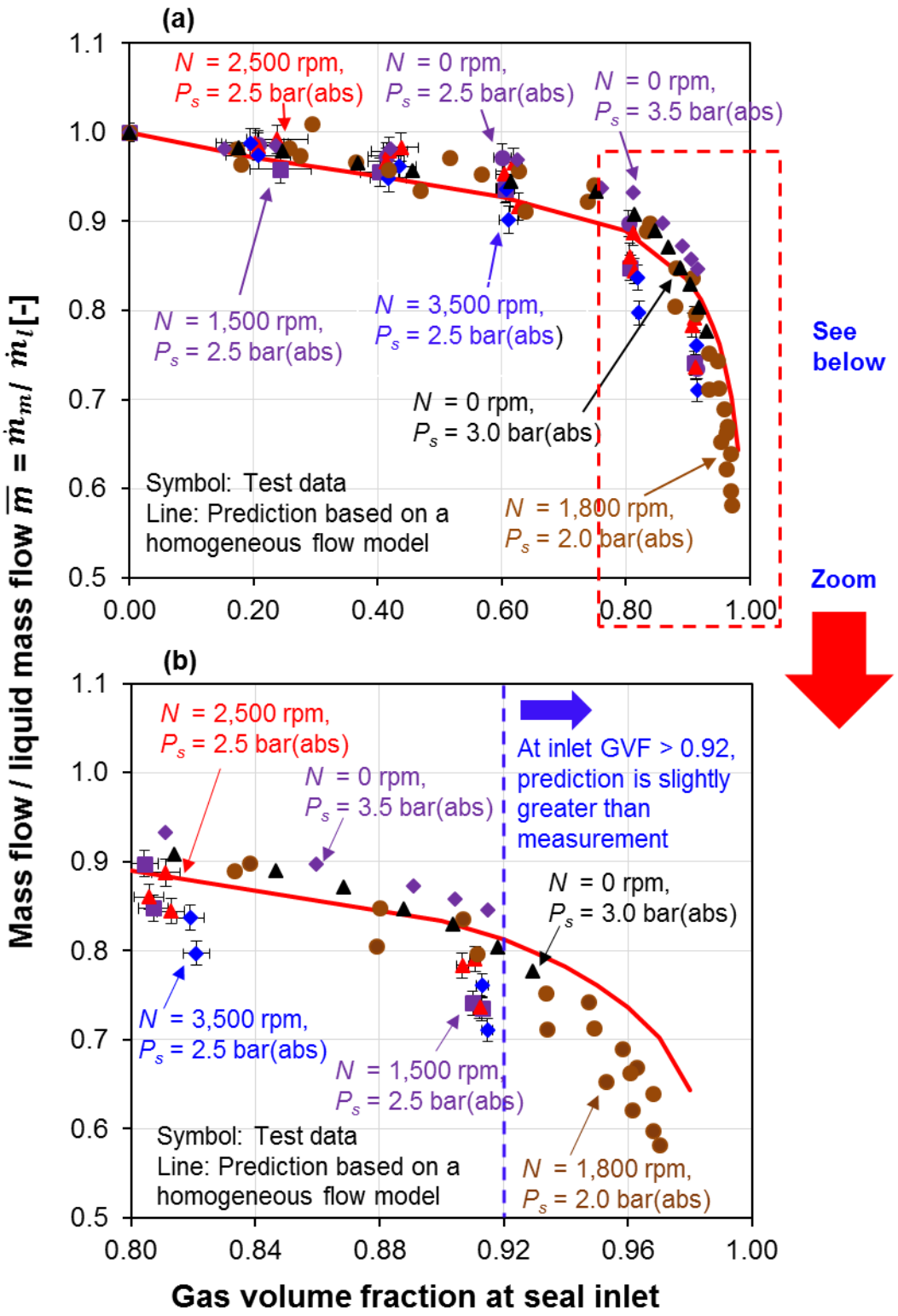

Figure 3. Normalized wet seal leakage ($\overline{m}_m$) vs. inlet GVF. Supply pressure (P_s) = 2.0, 2.5, 3.0, 3.5 bar (abs), discharge pressure (P_a) = 1 bar (abs), oil temperature (T_{in}) = 33 ºC~35 ºC. Shaft speed (N) = 0, 1,500, 1,800, 2,500, 3,500 rpm (ΩR = 23.3 m/s).

The single phase axial flow mean velocity at the seal inlet plane is $V_Z = Q / A_c$, where, Q is the inlet volumetric flow rate of a single phase and $A_c = \pi Dc$ is the area of axial flow. In a condition with inlet pressure (P_s) = 2.5 bar (abs), shaft speed (N) = 0 rpm, the oil inlet axial flow mean velocity (V_L) varies from 0.93 m/s ($\alpha_{inlet} = 0$) to 0.65 m/s ($\alpha_{inlet} = 0.9$), while the gas inlet flow mean velocity (V_G) varies 0 m/s ($\alpha_{inlet} = 0$) to 19 m/s ($\alpha_{inlet} = 0.9$).

For reference, Figure 4 shows a flow regime map for the flow of an air/oil mixture in a vertical 2.5-cm-diameter pipe. The graph adapted from Brennen (2005) [11] shows experimentally observed transition flow regions. The graph characterizes the flow in term of the components' velocities (gas vs. liquid). The red circles superimposed on the graph identify the mixture flow regime with supply pressure = 2.5 bar (abs), shaft speed = 0 rpm, and inlet gas volume fraction $0 < \alpha_{inlet} < 0.9$. The flow regime maps shows a transition from liquid flow, to bubbly flow, to churn and slug flow, to annular flow as the mixture gas volume fraction increases from 0 to 0.9.

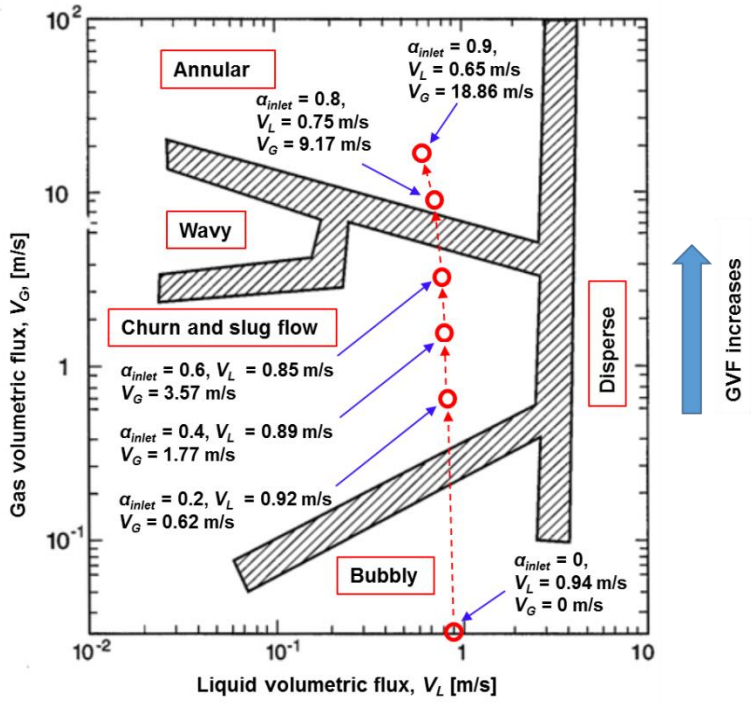

Figure 4. A flow regime map for an air/oil mixture in a vertical pipe with diameter 2.5 mm. Supply pressure (P_s) = 2.5 bar (abs), shaft speed (N) = 0 rpm. Adapted from Brennen, C. E., (2005) [11]. (Reproduced with permission from Adam Hirschberg, Senior Permissions Associate, Cambridge University Press).

SEAL DYNAMIC FORCE COEFFICIENTS

Force coefficient identification procedure

Dynamic load tests aim to assess the effect of mixture inlet GVF (α_{inlet}), shaft speed (N), supply pressure (P_s) and excitation frequency (ω) on the seal mechanical parameters, i.e., damping (C), stiffness (K), and mass (M) force coefficients.

Figure 5 shows a schematic view of a seal-journal assembly. The journal rotates at angular speed Ω. Identification of the seal force coefficients requires of multiple processes. First, single frequency (or other type) unidirectional load tests performed on the *dry* system[5] at zero speed serve to identify the structural stiffness (K_S), mass (M_S) and damping (C_S) coefficients. The instrumental variable filter method (IVF) [12] estimates the structural coefficients as K_S = 710 kN/m, M_S = 7.1 kg, C_S = 0.2 kN s/m. Note M_S = 6.7± 0.04 kg using a scale [1]. The dry system coefficients are referred to as "baseline" parameters. The estimated structural damping ratio ξ_S ~ 4.5% and the test system "dry" natural frequency ω_n = 50 Hz.

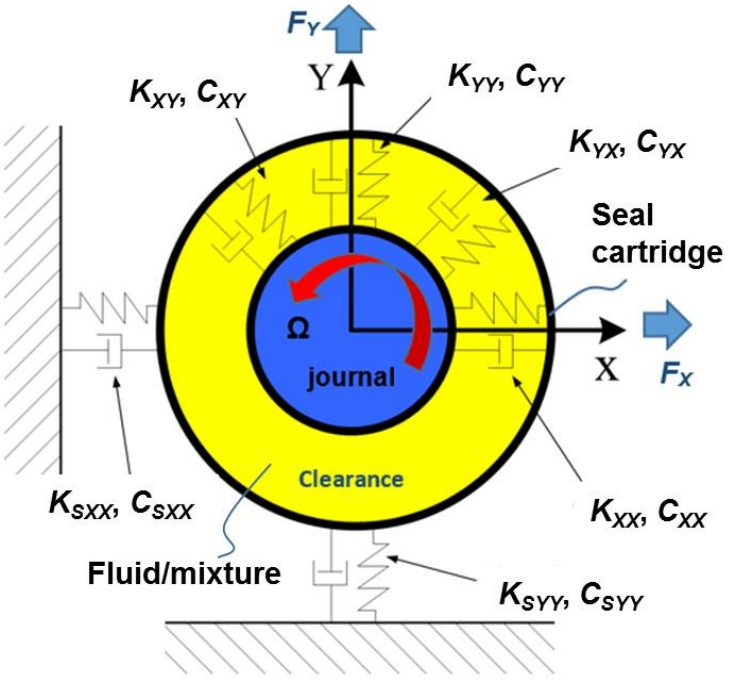

Figure 5. Schematic representation of seal-journal system with force coefficients and coordinate system [13]

[5] A dry system is a system without air or oil or mixture being supplied to the seal.

Next, with the seal lubricated by either a pure oil or an air in oil mixture with a known inlet GVF, and the shaft spinning at speed (*N)*, one shaker forces the seal cartridge (SC) to displace along the *X* direction with motion amplitude (*r*) and a single frequency (ω) that ranges from 30 Hz to 150 Hz. The other shaker (*Y* direction) is at rest. The sensors record the force $\mathbf{F_X} = [f_X = f_o\, \varepsilon^{\imath\omega t}, f_Y = 0]^T$, the ensuing relative displacement $\mathbf{z_X} = [X_X, Y_X]^T$, and the absolute SC acceleration $\mathbf{a_X} = [a_{XX}, a_{YX}]^T$. Then, shaker *X* stops and shaker *Y* repeats the force excitation. Similarly, the sensors record the force $\mathbf{F_Y} = [f_X = 0, f_Y = f_o\, \varepsilon^{\imath\omega t}]^T$, the ensuing relative displacement $\mathbf{z_Y} = [X_Y, Y_Y]^T$, and the absolute SC acceleration $\mathbf{a_Y}=[a_{XY}, a_{YY}]^T$.

There are18 sets of tests as listed in Table 3. Recall that in practice a multiphase pump must handle a flow with GVF up to 100% [2], conversely a *wet* gas centrifugal compressor needs to work with a flow with LVF up to 5% [4-5]. At the supply of 2.5 bar (abs), the Mach number at the seal exit plane is approximately 0.7. Tests for $\alpha_{inlet} = 1$ (pure gas) at P_s = 2.5 bar (abs) could not be conducted as choked flow may develop in the seal.

Table 3. Operating conditions for dynamic load tests conducted on *wet* seals. Supply pressure (P_s) = 2.5 bar(abs), discharge pressure (P_a) = 1 bar(abs), inlet temperature (T_{in}) = 33 ºC ~35 ºC.

Shaft speed, *N* (rpm)	Gas volume fraction at seal inlet GVF, [-]						
	0	0.2	0.4	0.6	0.8	0.9	1
0 (ΩR = 0 m/s)	√	√	√	-	-	-	-
2500 (ΩR = 16.6 m/s)	√	√	√	√	√	√	-
3500 (ΩR = 23.3 m/s)	√	√	√	√	√	√	-

San Andrés [13] details the parameter identification procedure in the frequency domain. Let $\mathbf{F}_{(\omega)} = [\mathbf{F_{X(\omega)}} \mid \mathbf{F_{Y(\omega)}}]$, $\mathbf{A}_{(\omega)} = [\mathbf{A_{X(\omega)}} \mid \mathbf{A_{Y(\omega)}}]$, $\mathbf{D}_{(\omega)} = [\mathbf{Z_{X(\omega)}} \mid \mathbf{Z_{Y(\omega)}}]$ be the force matrix, acceleration matrix and displacements in the frequency domain. The test system has a complex stiffness matrix given as

$$\mathbf{H}_{(\omega)} = [\mathbf{K} - \omega^2\mathbf{M} + \mathrm{i}\omega\mathbf{C}] = [\mathbf{F}_{(\omega)} - M_S\mathbf{A}_{(\omega)}]\, \mathbf{D}_{(\omega)}^{-1} \tag{3}$$

where $\mathrm{i} = \sqrt{-1}$.

The small amplitude of motion of the SC around the centered position ensures a linearized test system. In a *wet* seal, the mixture is compressible due to the gas content; hence the force coefficients are frequency dependent [9].

Subtracting the *dry* system force coefficients from the lubricated system force coefficients yields the seal dynamic complex stiffness $[\mathbf{H}]_{Seal} = [\mathbf{H}] - [\mathbf{K}]_s - i\omega[\mathbf{C}]_s$, thus

$$[\mathbf{K}]_{Seal} = \mathrm{Re}[\mathbf{(H)}] - [\mathbf{K}]_s \quad (4)$$

$$[\mathbf{C}]_{Seal} = \mathrm{Im}[\mathbf{(H)}] / \omega - [\mathbf{C}]_s \quad (5)$$

A past TRC report [1] details the uncertainty in the estimated physical parameters. In general, the uncertainty for the reported stiffness (K), damping (C) and mass (M) is $U_K <$ 4.1%, $U_C <$ 6.6% and $U_M <$ 8.5%. These uncertainties are valid over the frequency range 30 Hz to 150 Hz only.

Figure 6 shows an applied load and the ensuing SC response for $\alpha_{inlet} = 0$ and 0.2 at a frequency of 30 Hz. The graphs on the left (a) show the load and seal displacement response for operation with a pure oil, while the graphs on the right (b) show the load and seal motion for operation with an air in oil mixture with inlet GVF = 0.2, for example. The top graph in (a) shows the applied load along the X direction, the middle and bottom graphs show the response (Disp X and Y) induced by the excitation along the X and Y directions, respectively. Note that shaft rotation introduces considerable cross-coupled displacements.

During periodic load tests with shaft rotation, the seal displays motion with two main frequencies; one equals to the shaft angular speed (Ω), and the other equals the excitation frequency (ω). The motion synchronous with shaft angular speed (Ω) is circular and has an amplitude (e) = 27 μm (~ 15% of the seal radial clearance; c = 0.203 mm), as shown in the second graph of Figure 6 (a). The amplitude of the forced response at the excitation frequency 30 Hz is r = 8 ±1 μm (~ 5% of the seal radial clearance).

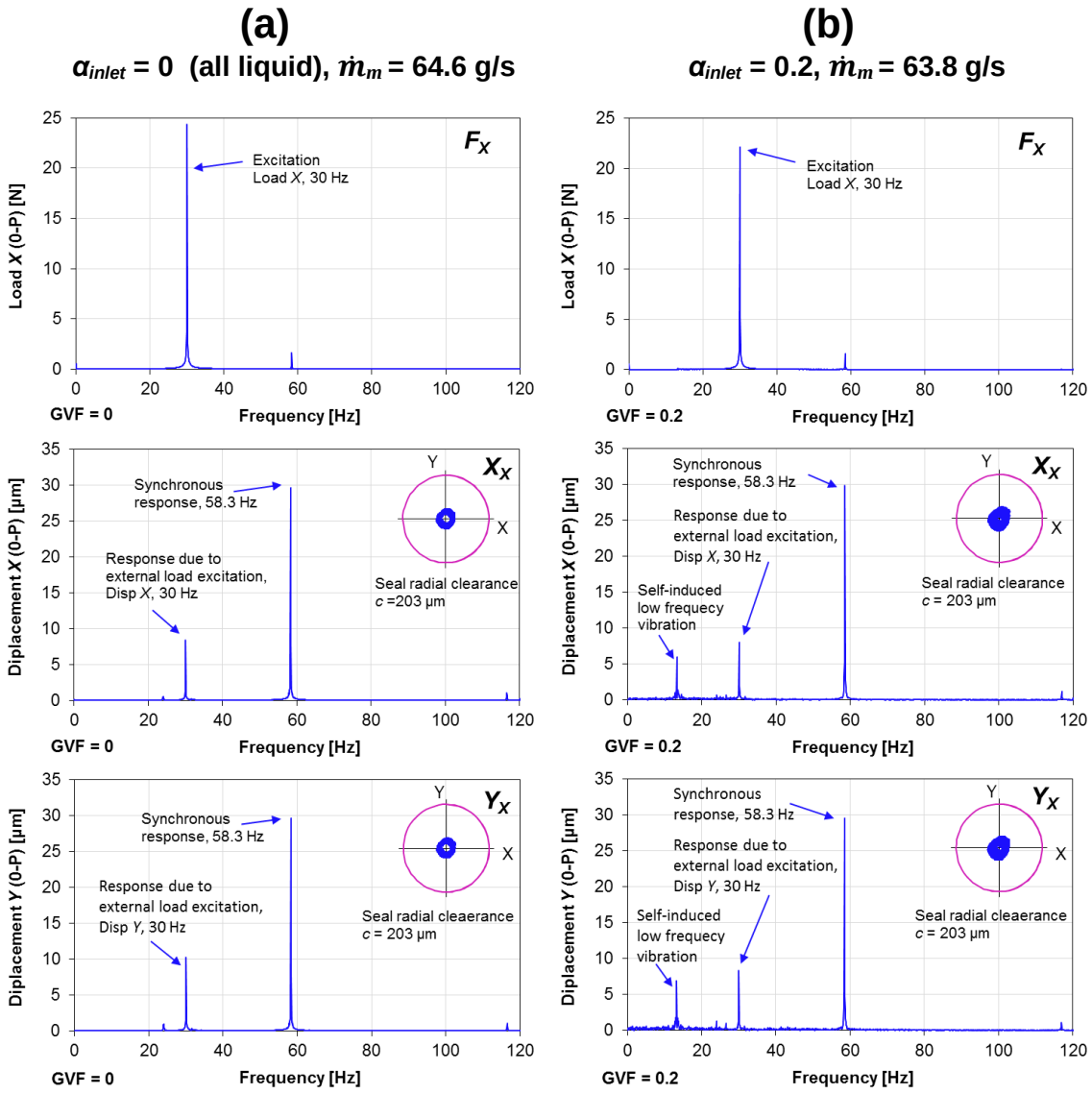

Figure 6. Seal cartridge dynamic response for test with (a) α_{inlet} = 0 and (b) α_{inlet} = 0.2. Supply pressure P_s =2.5 bar (abs), discharge pressure P_a = 1 bar (abs), oil temperature T_{in} = 33 ºC ~35 ºC. Journal speed 3500 rpm (58.3 Hz). External load (*X* direction) with frequency 30 Hz.

The injection of air into the flowing oil generates a two-component mixture and also introduces considerable noise into the test system. Under this condition, the seal shows a (self-induced) low frequency motion with frequency ranging from 8 Hz to 20 Hz. This frequency is different from the frequency of the synchronous response (1X) and the response induced by the external excitation. A latter section discusses this low frequency vibration phenomenon in more detail.

Real part Re(H) and imaginary part Im(H) of seal complex stiffness

Figure 7 shows the real part of the seal complex stiffness Re(H_{XX}) versus whirl frequency (ω) for operation at shaft speed (N) 3,500 rpm (58.5 Hz) and at a supply pressure (P_s) 2.5 bar (abs). The air in oil mixture has increasing inlet GVF. Table 4 shows the corresponding mixture mass flow rate ($\dot{m}_m$). The oil temperature (T_{in}) = 33 ~ 35 ^oC.

Table 4. Seal leakage ($\dot{m}_m$) for air in oil mixture. Supply pressure (P_s) = 2.5 bar (abs), discharge pressure (P_a) = 1 bar (abs), shaft speed (N) = 3,500 rpm (shaft surface speed ΩR = 23.3 m/s). Oil temperature (T_{in}) = 33 ^oC ~35 ^oC.

supply pressure, P_s (bar (abs))	shaft speed, N (rpm)	Inlet GVF (-)	Measured leakage, $\dot{m}_m$ (g/s)	Clearance c (mm)	Temperature T (^oC)	Oil viscosity, μ (cP)
2.5	3,500	0.0 0.2 0.4 0.6 0.8 0.9	68.0 ± 1.2 66.7 ± 0.7 65.0 ± 0.7 62.6 ± 2.3 55.6 ± 0.4 50.0 ± 0.8	0.203	34	10.6

In general, at a specific whirl frequency, i.e., ω = 70 Hz (10 Hz above the shaft speed), both Re(H_{XX}) and Re(H_{YY}) increase as the inlet GVF increases from 0 to 0.4. After reaching a peak at inlet GVF = 0.4, Re(H_{XX}) and Re(H_{YY}) drop as α_{inlet} increases further from 0.4 to 0.9. At a typical inlet GVF, for example, α_{inlet} = 0.9, Re(H_{XX}) and Re(H_{YY}) increase with whirl frequency (ω). For a pure oil condition, both Re(H_{XX}) and Re(H_{YY}) decrease with frequency (ω).

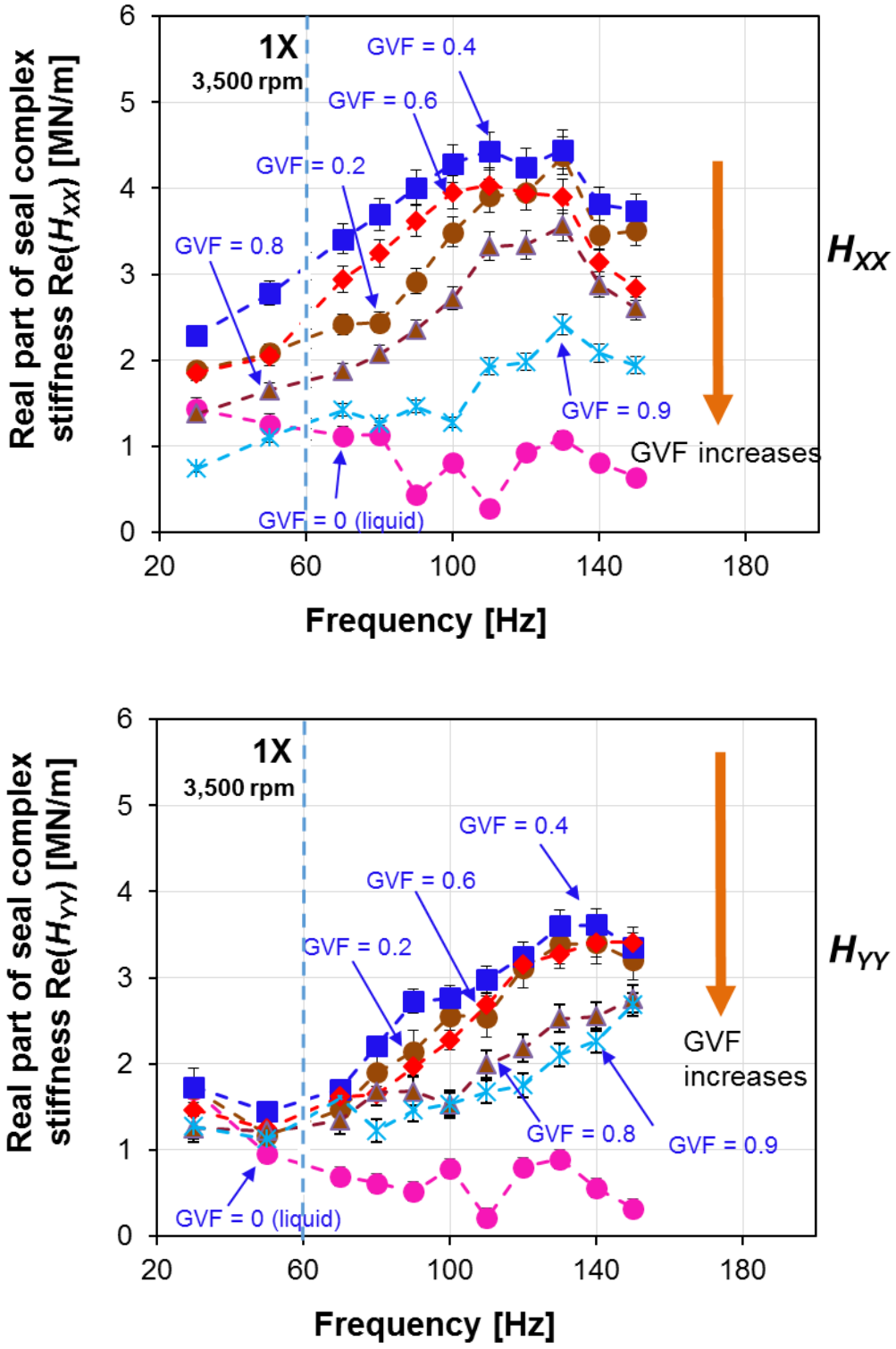

Figure 7. Real part of seal direct complex stiffness Re(H_{XX}) and Re(H_{YY}) vs. whirl frequency (ω). Inlet GVF varies from 0 to 0.9. Shaft speed (N) = 3,500 rpm. Supply pressure (P_s) = 2.5 bar (abs), discharge pressure (P_a) = 1 bar (abs), oil temperature (T_{in}) = 33 ºC ~35 ºC.

For operation with various inlet GVF, Figure 8 depicts the real part of the seal cross coupled complex stiffness Re(H_{XY}) and Re(H_{YX}) versus excitation frequency. The shaft speed (N) is 3,500 rpm, the inlet pressure (P_s) is 2.5 bar (abs), and the oil temperature is T_{in} = 33 ~ 35 ^{o}C.

Test results shows that Re(H_{XY}) and Re(H_{YX}) have opposing signs; both decreasing in magnitude as the excitation frequency (ω) increases. Note that at a specific inlet GVF = 0.2 for example, the cross coupled terms are comparable in magnitude to the direct dynamic stiffnesses as shown in Figure 7.

At a specific excitation frequency (ω) = 70 Hz, Re(H_{XY}) drops from 4.4 MN/m for a mixture with inlet GVF = 0 to 1.3 MN/m for another mixture with inlet GVF = 0.8. At a higher magnitude of inlet GVF > 0.8, a further increase in inlet GVF drops little the cross coupled stiffnesses.

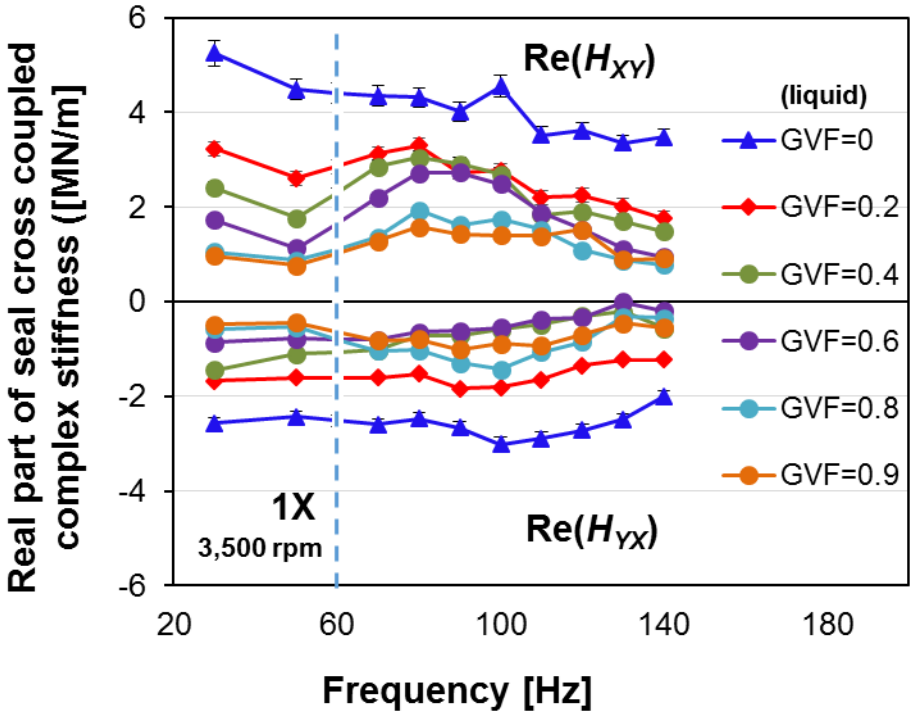

Figure 8. Real part of seal cross coupled complex stiffness (Re(H_{XY}) and (Re(H_{YX})) vs. whirl frequency (ω). Inlet GVF varies from 0 to 0.9. Shaft speed (N) = 3,500 rpm. Supply pressure (P_s) = 2.5 bar (abs), discharge pressure (P_a) = 1 bar (abs), oil temperature (T_{in}) = 33 ^{o}C ~35 ^{o}C.

For operation at 3,500 rpm and an air in oil mixture with increasing inlet GVF, Figure 9 shows the imaginary part of the seal complex stiffness (a) Im(H_{XX}) and (b) Im(H_{YY}). The line is a curve fit for ωC_{Seal} for a liquid condition ($\alpha_{inlet} = 0$) only.

At an inlet GVF = 0, both Im(H_{XX}) and Im(H_{YY}) increase proportionally with whirl frequency (ω). As gas is injected to make a mixture, the imaginary part of H is no longer proportional to frequency, and cannot be characterized by a constant viscous damping (C), i.e., Im(H) $\neq \omega C$. At an excitation frequency of 70 Hz, an increase in inlet GVF decreases significantly Im(H_{XXl}) and Im(H_{YYl}), for example.

In Figure 9, graphs (a) and (b) show Im(H_{XX}) > Im(H_{YY}). This is because the seal cartridge becomes slightly off centered along the X direction when the seal is lubricated with either a pure oil or an air in oil mixture. Note in Figure 7 Re(H_{XX}) > Re(H_{YY}) as well.

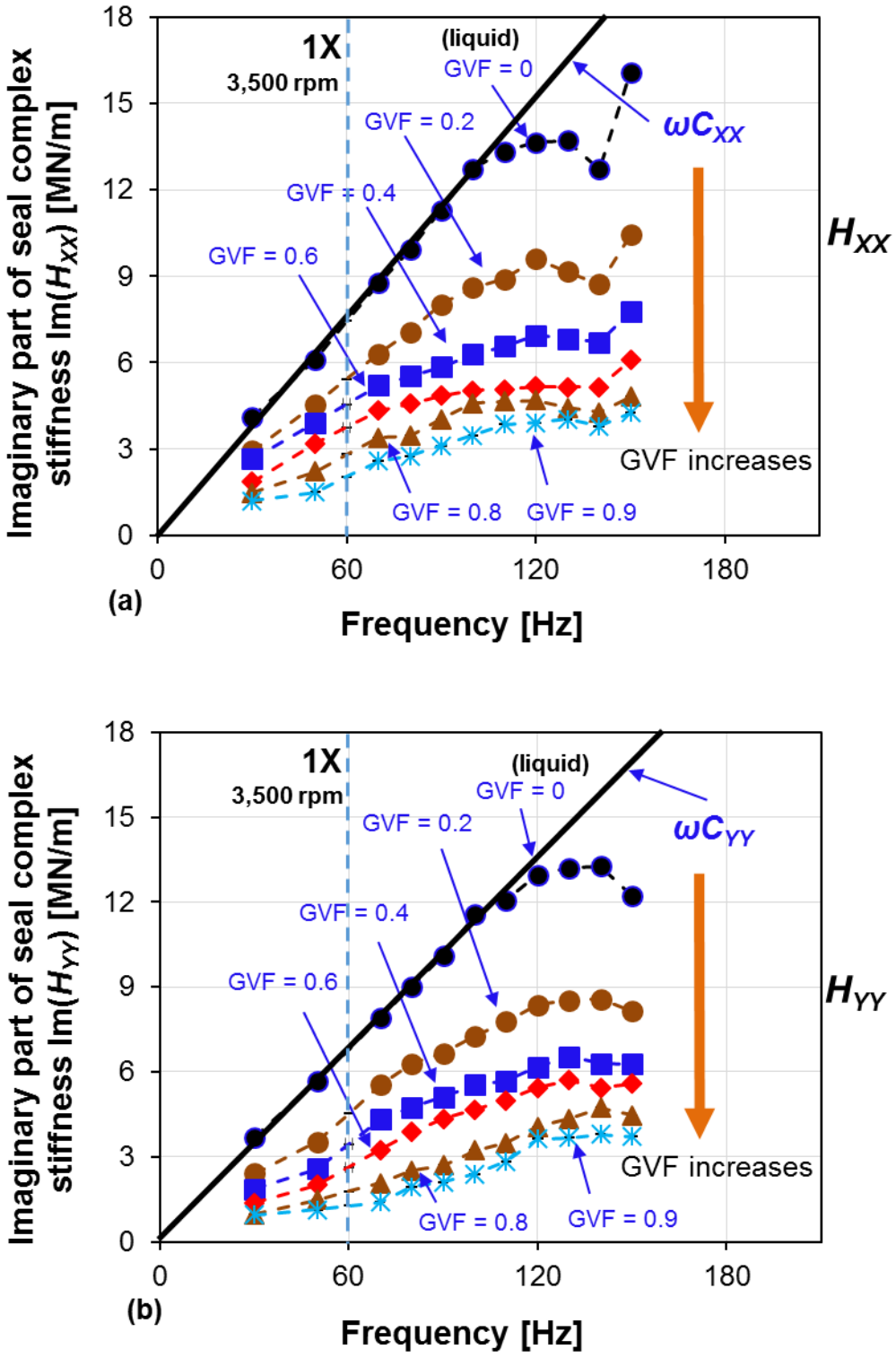

Figure 9. Imaginary part of seal complex stiffness (Im(H_{XX}) and Im(H_{YY})) vs. whirl frequency (ω). Inlet GVF varies from 0 to 0.9. Shaft speed (N) = 3,500 rpm. Supply pressure (P_s) = 2.5 bar (abs), discharge pressure (P_a) = 1 bar (abs), oil temperature (T_{in}) = 33 ºC ~35 ºC.

Seal cross coupled stiffnesses (K_{XY}, K_{YX}) and direct damping coefficients (C_{XX} and C_{YY})

For operation at supply pressure (P_s) = 2.5 bar (abs) and an air in oil mixture with increasing inlet GVF = 0 to 0.9, Figure 10 shows the seal cross coupled stiffness ($K_{XY} \leftarrow$ Re(H_{XY}) and $K_{YX} \leftarrow$ Re(H_{YX})) versus frequency (ω) and two shaft speeds (N) (top) 2,500 and (bottom) 3,500 rpm. The cross coupled stiffnesses at zero shaft speed are negligible and not shown here.

At a specific inlet GVF, the cross coupled stiffness in graph (b) (3,500 rpm) is greater than the one in graph (a) (2,500 rpm). For example, at a typical magnitude of inlet GVF = 0 (pure oil), $K_{XY(3500rpm)}/\ K_{XY(2500rpm)}$ = 1.4, $K_{YX(3500rpm)}/\ K_{YX(2500rpm)}$ = 1.44. This is similar to the shaft speeds' ratio 3500 rpm/2500 rpm = 1.4.

When the seal operates with an air in oil mixture, the ratio of $K_{XY(3500rpm)}/\ K_{XY(2500rpm)}$ decreases. For example, at 70 Hz, the ratio of $K_{XY(3500rpm)}/\ K_{XY(2500rpm)}$ decreases from 1.4 at inlet GVF = 0 to nearly 1.0 at inlet GVF = 0.6. As inlet GVF > 0.6, the increase of shaft speed from 2,500 rpm to 3,500 rpm changes little the magnitude of cross coupled stiffnesses.

Over the whole frequency range of 0 to 150 Hz, when operating with an air in oil mixture, the seal cross coupled stiffnesses decrease as the frequency (ω) increases for operation at both shaft speeds (2,500 rpm and 3,500 rpm).

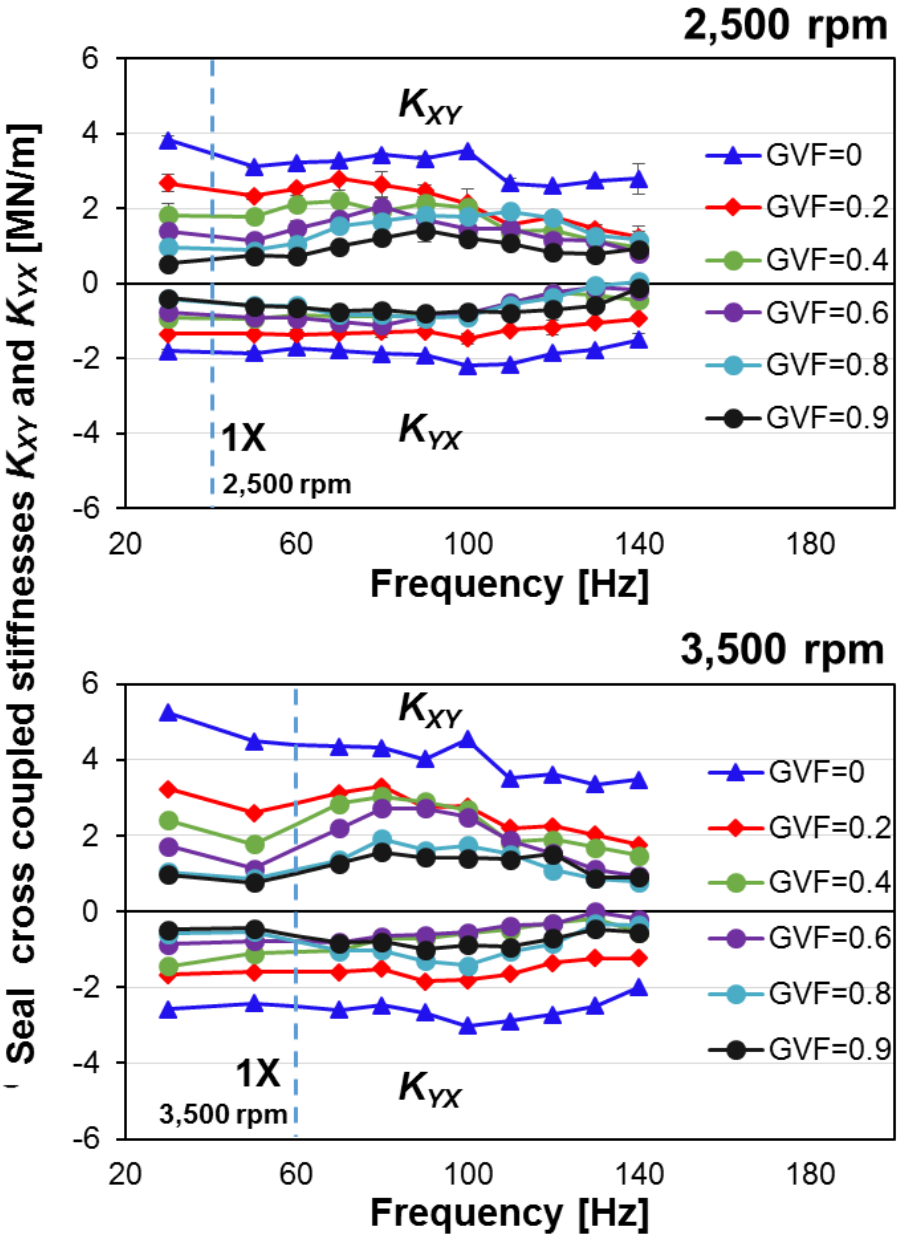

Figure 10. Seal cross coupled stiffness (K_{XY} and K_{YX}) vs. whirl frequency (ω). Inlet GVF varies from 0 to 0.9. Shaft speed (N) = 2500 rpm (ΩR = 16.6 m/s) and 3500 rpm (ΩR = 23.3 m/s). Supply pressure (P_s) = 2.5 bar (abs), discharge pressure (P_a) = 1 bar (abs), inlet temperature (T_{in}) = 33 ºC ~35 ºC

For operation at shaft speed (N) = 0, 2,500 and 3,500 rpm, supply pressure (P_s) = 2.5 bar (abs) and an air in oil mixture with increasing inlet GVF = 0 to 0.9, Figure 11 shows the seal direct damping: (a) C_{XX} = Im(H_{XX})/ω and (b) C_{YY} = Im(H_{YY})/ω. The symbols represent test data and the line stands for a predicted direct damping for a seal operating with a non-spinning journal and lubricated with pure oil. Error bars on the vertical axis show the variability of the damping coefficients.

The seal direct damping (C) shown in Figure 11 decreases continuously with an increase in the inlet GVF. At a shaft speed of 2,500 rpm, the seal direct damping C_{XX} decreases from 22 kN.s/m for a mixture α_{inlet} = 0 to 6 kN.s/m with α_{inlet} = 0.9. Note for a laminar flow incompressible liquid flowing through the seal, the estimated damping is $C_L = \pi\mu_l R(L/c)^3$ = 24.6 kN.s/m [14].

The direct damping (C_{XX} and C_{YY}) becomes frequency (ω) dependent with air content in the oil, and the damping decreases steadily with the increase in excitation frequency at a specific GVF and shaft rotational speed (N). For example, at inlet GVF = 0.2 and shaft speed (N) = 2,500 rpm, C_{XX} and C_{YY} drop steadily as frequency (ω) increases. However, for a condition with inlet GVF = 0.8 and 0.9, and over the frequency range 30 Hz < ω < 120 Hz, C_{XX} and C_{YY} change little with frequency (ω).

The influence of shaft speed (N) on the magnitude of the seal direct damping (C_{XX}, C_{YY}) is significant for an inlet GVF < 0.4. For example, with a pure oil condition (α_{inlet} = 0), C_{XX} drops from 24.6 kNs/m at 0 rpm, to 21 kN.s/m at 2,500 rpm to 19 kN.s/m at 3,500 rpm. At an inlet GVF > 0.4, the effect of shaft speed on the seal direct damping is minor.

Recall the seal operates in a laminar flow condition. The increase of shaft speed intensifies the shear drag that generates more heat inside the seal clearance. The more heat there is, the higher the oil temperature (inside the seal) will be. The increase of oil temperature drops the mixture viscosity (μ_m) and increases the seal clearance (c), and hence these two changes affect the generation of damping, $C \sim \mu_m/c^3$.

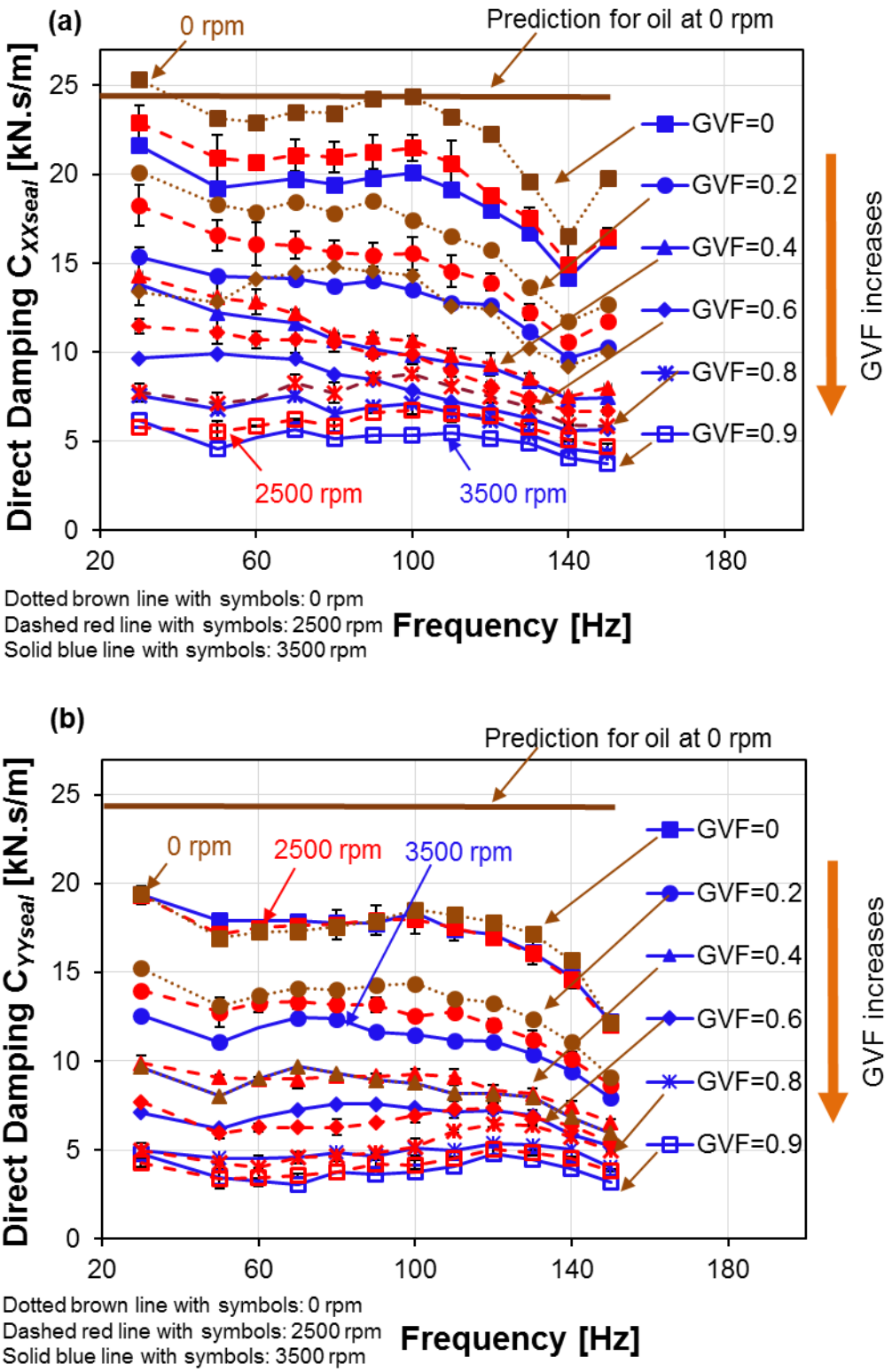

Figure 11. Experimental seal direct damping coefficient (C_{XX} and C_{YY}) vs. whirl frequency (ω). Inlet GVF varies from 0 to 0.9. Supply pressure (P_s) = 2.5 bar (abs), discharge pressure (P_a) = 1 bar (abs), inlet temperature (T_{in}) = 33 ºC ~35 ºC. Journal speed (N) = 0 rpm, 2500 rpm, 3500 rpm.

Effective damping coefficients (C_{XXeff} and C_{YYeff})

At a shaft speed of 2,500 rpm, supply pressure of 2.5 bar (abs), and operating with an air in oil mixture, Figure 12 shows the seal effective damping coefficients:

$$C_{XXeff} = C_{XX} - \frac{K_{XY}}{\omega} \tag{6}$$

$$C_{YYeff} = C_{YY} + \frac{K_{YX}}{\omega} \tag{7}$$

The effective damping (C_{XXeff} and C_{XXeff}) increase over the range $0 < \omega < 110$ Hz, and decreases after 110 Hz. At a specific whirl frequency (ω), the effective damping decreases with an increase in the inlet GVF. The mixture with more liquid content has greater viscosity (μ_m) to generate more damping.

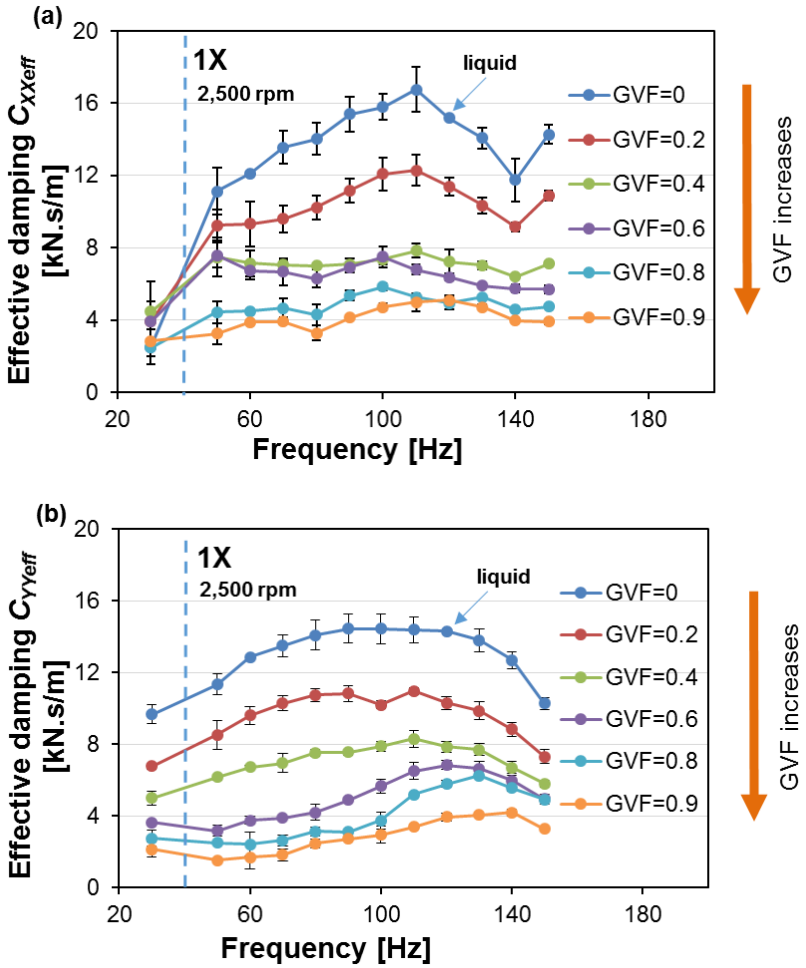

Figure 12. Effective damping coefficients (C_{XXeff} and C_{YYeff}) vs. whirl frequency (ω). Inlet GVF varies from 0 to 0.9. Supply pressure (P_s) = 2.5 bar (abs), discharge pressure (P_a) = 1 bar (abs), inlet temperature (T_{in}) = 33 ºC ~35 ºC. Journal speed (N) = 2500 rpm.

SEAL LOW FREQUENCY VIBRATION

Description of low frequency vibration phenomenon

Recall Figure 6 shows an unusual subsynchronous vibration for operation with an air in oil mixture. This section discusses this low frequency motion in more detail.

Figure 13 portrays cross sections of the seal test showing eddy current displacement sensors and piezoelectric dynamic sensors. In the *X*-*Z* plane, two piezoelectric dynamic pressure sensors (P_1 and P_2) installed 12.7 mm and 30.5 mm downstream of the seal inlet plane measure the film dynamic pressure during operation. Incidentally, a displacement sensor measures the relative motion of the seal cartridge. The displacement sensor and dynamic sensors are installed 180° apart as shown in cross section A-A.

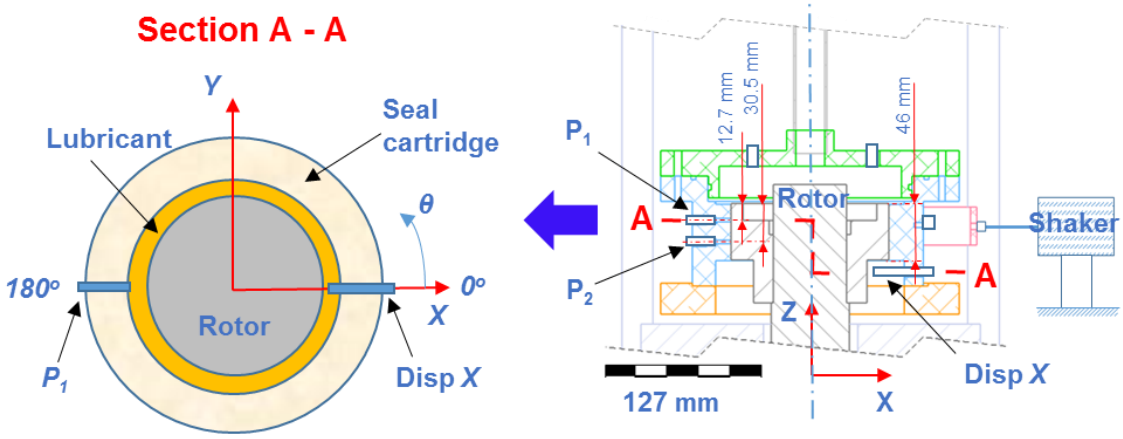

Figure 13. Cross sections of test rig (top and side) showing two dynamic pressure sensors (P_1 and P_2), a displacement eddy current sensor (Disp *X*), and a shaker along the *X* direction.

For operation with pure oil (α_{inlet} = 0) and an air in oil mixture (α_{inlet} = 0.6), Figure 14 depicts the film pressure (P_1) and displacement (Disp *X*). The graph on the left show the pressure and displacement in the time domain, and the graph on the right show the pressure and displacement in the frequency domain. There is no external forced excitation induced by shaker.

For pure oil condition as shown in Figure 14 (a), both P_1 and *Disp X* show a magnitude of zero, indicating there is no dynamic pressure developed by the oil.

Figure 14 (b) depicts a pressure profile for operation with a mixture with an inlet GVF = 0.6. The dynamic pressure (P_1) fluctuates between -1 psi and 1 psi. Note the pressure profile is 180° out of phase with Disp *X* because the sensors are on opposite sides of the

SC. An increase in dynamic pressure (P_1) represents an increase in fluid reaction force acting on the SC towards the – X direction, which displaces the SC to the – X direction. The clearance at θ = 0° decreases accordingly. Thus the measured relative displacement (Disp X) decreases. The absence of external excitation (shaker is off) evidences this dynamic pressure is induced by the air in oil mixture. The force originated from the self-induced dynamic pressure causes the motion of the SC. Note the right graph of (b) show motion and pressure oscillation at frequency low than 10 Hz.

For comparison, a forced responses test is conducted for operation with an air in oil mixture with inlet GVF = 0.6 and a forced excitation at 80 Hz along the X direction. Figure 15 shows the SC motion (Disp X) and the dynamic pressure (P_1). The right graph shows (i) response of both the displacement and pressure at the excitation frequency of 80 Hz and (ii) the broad band low frequency vibration (< 10 Hz). In the zoomed graph of Figure 15, the dynamic pressure (P_1) is in phase with the displacement (Disp X).

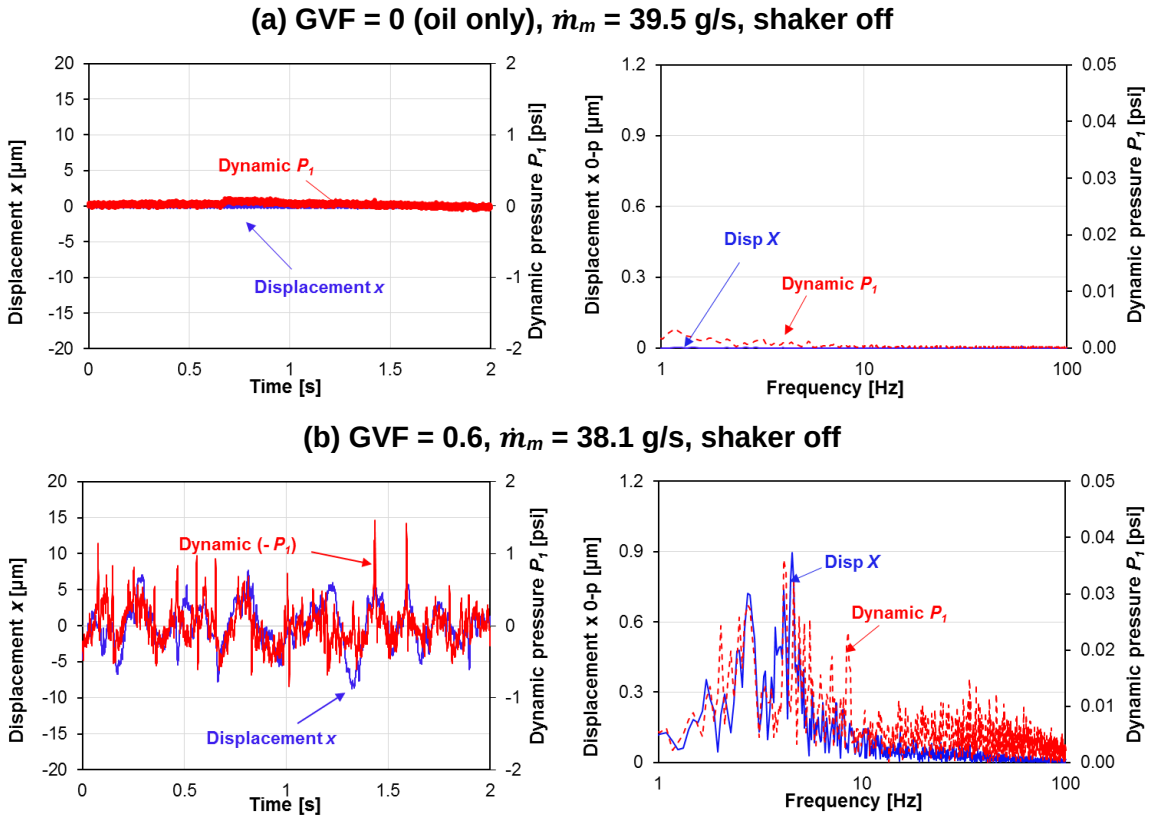

Figure 14. Self-induced dynamic pressure and seal displacement X: (a) inlet GVF = 0, (b) inlet GVF = 0.6. Shaker off. No shaft rotation. Supply pressure (P_s) = 2.0 bar (abs), discharge pressure (P_a) = 1 bar (abs), inlet temperature (T_{in}) = 33 ºC ~35 ºC.

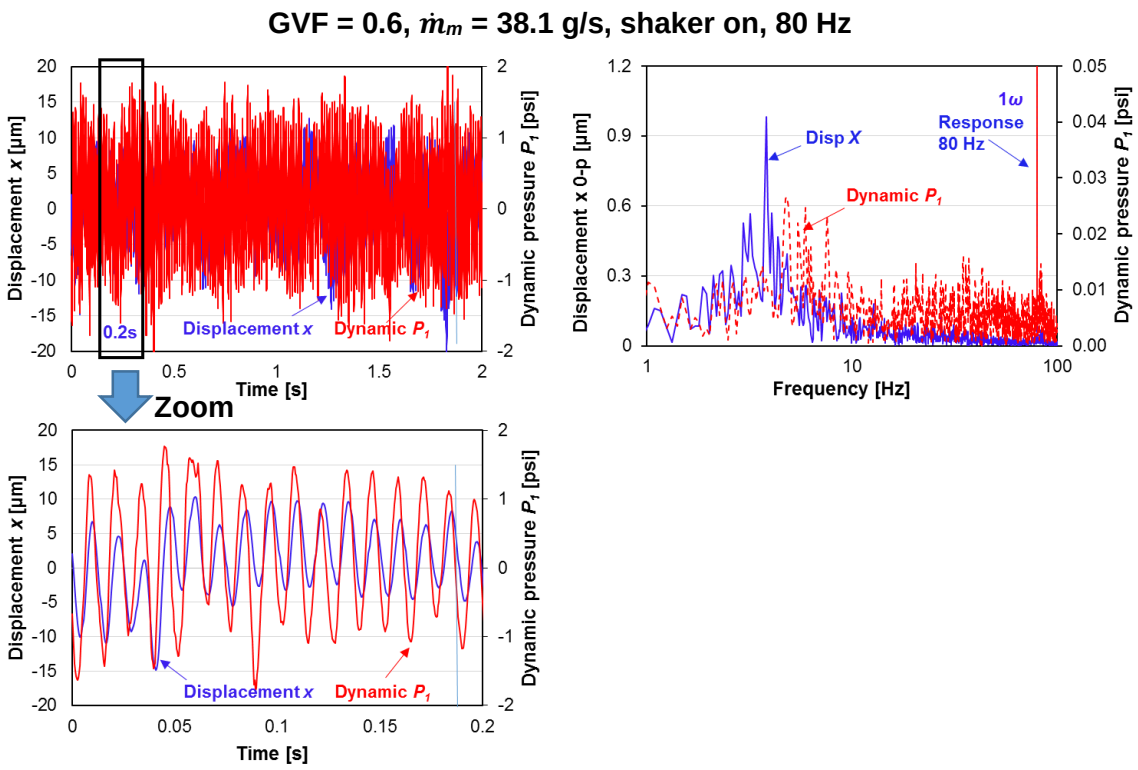

Figure 15. Forced dynamic pressure and seal forced displacement X. Inlet GVF = 0.6, shaker on with excitation at 80 Hz along the X direction. No shaft rotation. Supply pressure (P_s) = 2.0 bar (abs), discharge pressure (P_a) = 1 bar (abs), inlet temperature (T_{in}) = 33 ºC ~35 ºC.

For operation with a pure oil ($\alpha_{inlet} = 0$) and an air in oil mixture ($\alpha_{inlet} = 0.2 \rightarrow 0.9$), a supply pressure of 2.5 bar (abs), with shaft speed at 3,500 rpm (58.3 Hz), and a dynamic load at 80 Hz, Figure 16 shows cascade plots of the relative motion *Disp X*.

In Figure 16(a), for operation with a pure oil ($\alpha_{inlet} = 0$), the *Disp X* signal contains two main frequencies. One is synchronous (1X) with the shaft rotational speed 3,500 rpm (58.3Hz), and the other one coincides with the excitation frequency ω (80Hz).

While operating with an air in oil mixture with inlet GVF = 0.2, as shown Figure 16(b), an additional low frequency at ~12.3 Hz appears besides the two expected main frequencies (1X and 1ω). The amplitude of SC motion at this low frequency is approximately 7 μm.

Figure 16(c) shows the SC motion for operation with an air in oil mixture with inlet GVF = 0.4. The low frequency motion covers a broad band of frequencies. But a clear peak at 12.3 Hz can still be identified.

For $\alpha_{inlet} = 0.6$, shown in Figure 16(d), the low frequency motion spans a frequency range of 0 to 20 Hz with low amplitude, no clear peak can be identified under this condition.

A further increase of inlet GVF to 0.8, Figure 16(e) shows the seal displacement grows in both frequency and amplitude compared with operation conditions with lower inlet GVFs.

Lastly, for inlet GVF = 0.9, as depicted in Figure 16(f), the SSV grows further in both frequency range and amplitude. Note that the amplitude of low frequency motion is comparable in magnitude with that of the synchronous response. Besides the low frequency motion, vibrations at higher frequencies are also apparent.

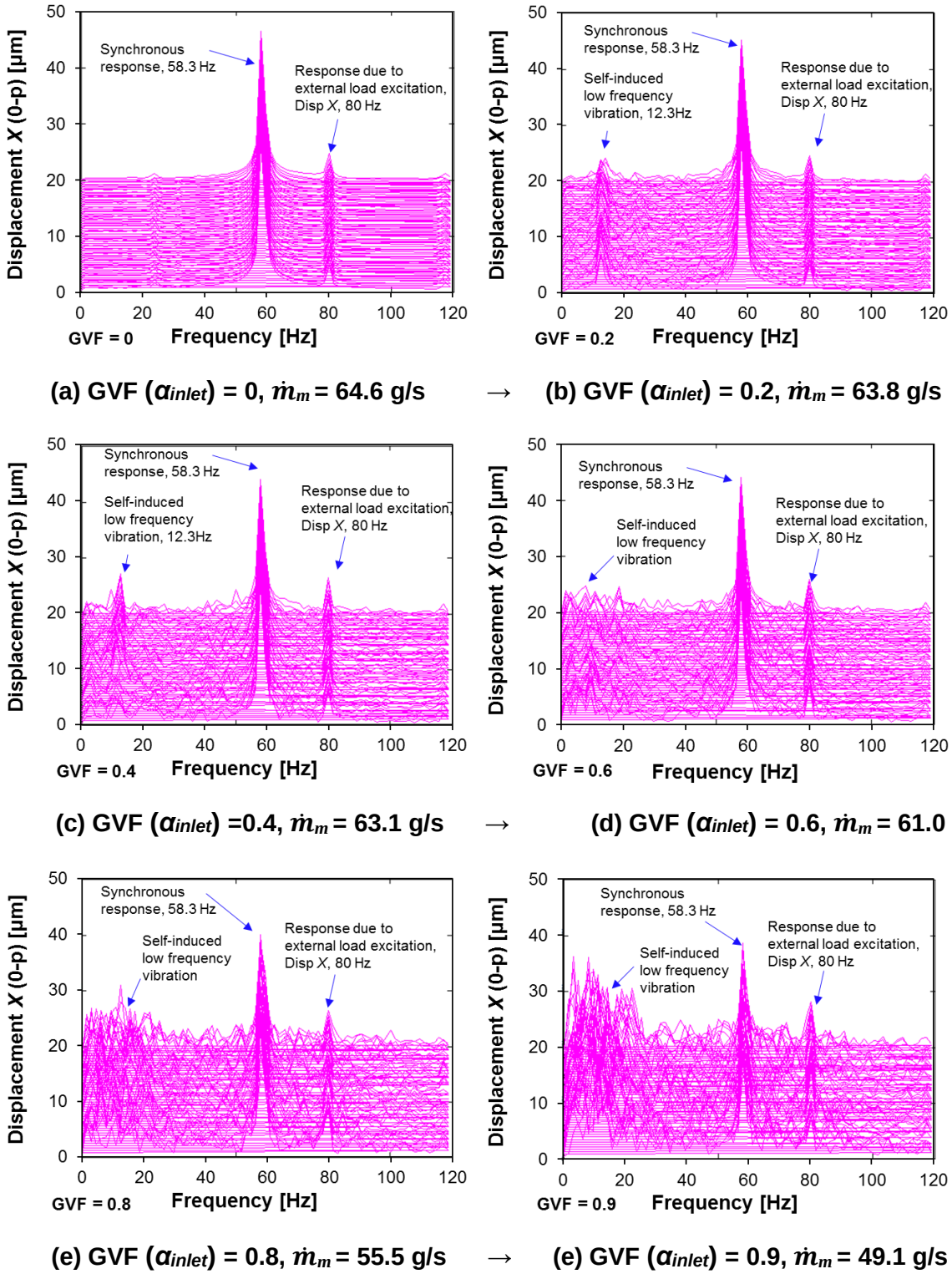

(a) GVF (α_{inlet}) = 0, $\dot{m}_m$ = 64.6 g/s → (b) GVF (α_{inlet}) = 0.2, $\dot{m}_m$ = 63.8 g/s

(c) GVF (α_{inlet}) =0.4, $\dot{m}_m$ = 63.1 g/s → (d) GVF (α_{inlet}) = 0.6, $\dot{m}_m$ = 61.0

(e) GVF (α_{inlet}) = 0.8, $\dot{m}_m$ = 55.5 g/s → (e) GVF (α_{inlet}) = 0.9, $\dot{m}_m$ = 49.1 g/s

Figure 16. Spectra of seal cartridge response (Disp *X*). (a) GVF = 0; (b) GVF = 0.2; (c) GVF = 0.4; (d) GVF = 0.6; (e) GVF = 0.8; (f). GVF = 0.9. Tests with a supply pressure (P_s) = 2.5 bar (abs), ambient pressure (P_a) = 1bar (abs), inlet temperature 33ºC ~35ºC. Journal speed 3,500 rpm (58.3 Hz), external load excitation frequency 80Hz.

Figure 17 shows two graphs describing trajectories of the SC for operation with: (a) a pure oil and (b) an air in oil mixture with inlet GVF = 0.8. It is quite obvious that an irregular orbit evolves for operation at inlet GVF = 0.8 compared with the circular motion for operation with a pure oil (GVF = 0).

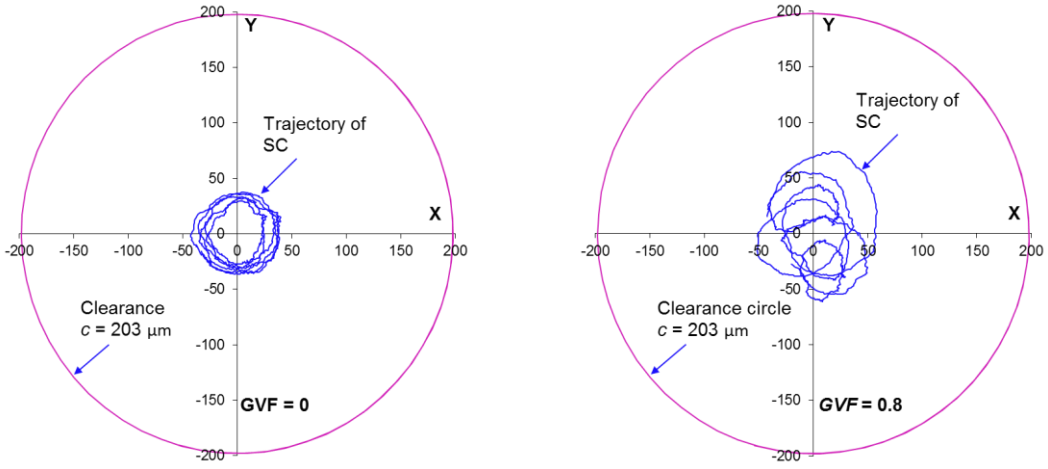

(a) GVF(α_{inlet}) = 0, $\dot{m}_m$ = 64.6 g/s **(b) GVF(α_{inlet}) = 0.8, $\dot{m}_m$ = 55.5 g/s**

Figure 17. Trajectory of SC (5 cycles 1X in each graph). (a) *GVF* = 0; (b) *GVF* = 0.8. Tests with a supply pressure (P_s) = 2.5 bar (abs), ambient pressure (P_a) = 1 bar (abs), inlet temperature 33°C ~35°C. Journal speed 3500 rpm, external load excitation with frequency 80Hz.

Possible source of low frequency motion

A single spherical bubble dispersed in an inviscid liquid has a natural frequency (ω_o) [15]

$$\omega_0 \simeq \frac{1}{R_B}\left(\frac{3P_0}{\rho_l}\right)^{1/2} \tag{8}$$

where P_0 is the liquid ambient pressure, R_B is the bubble radius, and ρ_l is the liquid density. With a pressure P_0 = 1 bar (abs), a radius R_B = 0.1 mm (equals half of the seal clearance 0.203 mm) and liquid density ρ_l = 1000 kg/m^3, the bubble natural frequency (ω_o) is approximately 27.6 kHz.

Bubbles in a cloud behave as coupled oscillators and may excite normal modes of the cloud itself at a substantially lower frequency than that of the individual constituent bubbles.

Lu and Prosperetti (1990) [15] derived a simple equation that correlates the cloud natural frequency with the bubble size and bubble number:

$$\frac{\omega_k}{\omega_0} \simeq \frac{k}{(\alpha^{1/2} N_B)^{1/3}} \tag{9}$$

where k = 1 represents the lowest natural frequency, α is the mixture gas volume fraction, and N_B is the number of gas bubbles in the cloud.

Assuming all the bubbles in the seal have equilibrium radius of R_B = 0.1 mm (the bubble diameter equals the seal clearance 0.203 mm), a mixture with GVF (α) = 0.4 will have number of bubbles $N_B = \alpha \cdot \frac{\text{Total Volume}}{\text{Single bubble volume}} = \alpha \cdot \frac{\pi DcL}{4\pi R_B^3/3}$ =35612. The lowest natural frequency is 453 Hz, which is 1/61 (453/27.6 k) of the natural frequency of a single bubble!

Note the calculation assumes all the bubbles are spherical and have the same radius (R_B) = 0.1 mm. In reality, the bubbles trapped in the seal clearance may not be spherical and can have large radius. As shown in Figure 18, the graph on left show the air in oil mixture for inlet GVF = 0.4. The bubble size can be as large as 4.1 mm. The graph on right depicts a mixture with α_{inlet} = 0.8 in which the gas bubbles travelling in groups.

Bubbles with larger size show lower natural frequencies. A set of bubble clouds consist of large size bubbles drops further the lowest natural frequency. Consequently, the seal may show low frequency motions as discussed above.

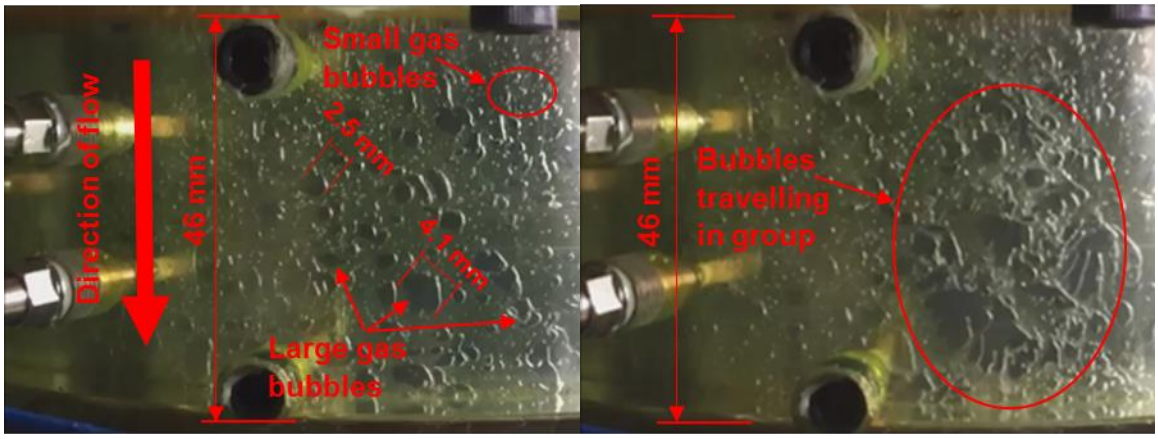

(a) GVF (α_{inlet}) =0.4, $\dot{m}_m$ = 63.1 g/s **(b) GVF (α_{inlet}) = 0.8, $\dot{m}_m$ = 55.5 g/s**

Figure 18. Air in oil mixture showing different size of gas bubbles in the seal clearance. Supply pressure (P_s) = 2.5 bar (abs), ambient pressure (P_a) = 1 bar (abs), inlet temperature 33ºC ~35ºC. No journal speed, shakers off.

CONCLUSION

The report shows measurements of leakage and dynamic force coefficients for an annular seal (L/D = 0.36) supplied with an air in ISO VG 10 oil mixture. The mixture delivered into a chamber at a supply pressure (P_s) in the seal cartridge, flows through the seal clearance (c), and discharges into a plenum at an ambient pressure (P_a).

In tests for seal leakage, the operation conditions are supply pressure (P_s) = 2.0, 2.5, 3.0, 3.5 bar (abs), discharge pressure (P_a) = 1 bar (abs), oil temperature (T_{in}) = 33 ~ 35 ^oC, shaft speed (N) = 0, 1,500, 1,800, 2,500, 3,500 rpm (ΩR = 23.3 m/s), and a mixture with increasing GVF = 0 to 0.97. Test results evidence the seal operates under laminar flow for operations with either a pure oil or an air in oil mixture. At a specific shaft speed, the mixture mass flow rate ($\dot{m}_m$) decreases steadily with the increase of inlet gas volume fraction (GVF). For a shaft speed range of 0 → 3,500 rpm (ΩR = 23.3 m/s), the shaft speed has negligible influence on the seal leakage.

In dynamic load tests over a frequency range of 30 to 150 Hz, the supply pressure (P_s) = 2.5 bar (abs), discharge pressure (P_a) = 1 bar (abs), inlet temperature (T_{in}) = 33 ^oC ~35 ^oC, journal speed (N) = 0 rpm, 2500 rpm, 3500 rpm. With gas content, the seal direct stiffnesses (K_{XX} and K_{YY}) increase with whirl frequency (ω). The virtual mass (M) cannot be obtained from a curve fit of Re(H) → $\omega^2 M$. The seal cross coupled stiffnesses (K_{XY} and K_{YX}) and direct damping (C_{XX} and C_{YY}) coefficient decrease continuously with an increase in the inlet GVF. The effective damping coefficients C_{XXeff} and C_{XXeff} increase with whirl frequency as $0 < \omega < 110$ Hz, and decrease as $110 < \omega < 150$ Hz. An increase in GVF drops the seal effective damping.

As air is injected into a flowing oil stream, for inlet gas volume fraction 0 < GVF < 0.6, the air in oil mixture generates a dynamic pressure wave that excites the seal cartridge at a typical frequency lower than 20 Hz. This slow motion develops into a broad band frequency vibration at inlet GVF > 0.6. Likely, bubble clouds emit acoustic waves that oscillate at low frequencies cause the low frequency motion.

REFERENCES

[1] San Andrés, L., Liu, Q., and Lu, X., 2015, “Measurements of Leakage and Estimation of Force Coefficients in a Short Length Annular Seal Operating Supplied with a Liquid/Gas Mixture (Stationary Journal),” Annual Report to the TAMU Turbomachinery Research Consortium, TRC-Seal-01-15, Texas A&M University (available for public release on May 2016).

[2] Gong, H., Falcone, G., et al., 2012, "Comparison of Multiphase Pumping Technologies for Subsea and Downhole Applications," Oil and Gas Facilities, pp. 36-46.

[3] Iwatsubo, T., and Nishino, T., 1993, “An Experimental Study on the Static and Dynamic Characteristics of Pump Annular Seals,” Proceedings of the 7th Workshop on Rotordynamic Instability Problems in High Performance Turbomachinery, Texas A&M University, College Station, TX, May 10–12.

[4] Brennen, L., Bjorge, T., Gilarranz, J., 2005, "Performance Evaluation of a Centrifugal Compressor Operating Under *Wet* Gas Conditions," Proceedings of the 34th Turbomachinery Symposium, Houston, TX, September 12-15.

[5] Vannini, G., Bertoneri, M., Del Vescovo, G. and Wilcox, M., 2014, “Centrifugal Compressor Rotordynamics in *Wet* Gas Conditions,” Proceedings of the 43rd Turbomachinery & 30th Pump Users Symposia, Houston, TX, September 23-25.

[6] Bertoneri, M., Wilcox, M., Toni, L. and Beck, G., 2014, “Development of Test Stand for Measuring Aerodynamic, Erosion, and Rotordynamic Performance of a Centrifugal Compressor under *Wet* Gas Conditions,” ASME Paper GT2014-25349

[7] Vannini, G., et al, 2016, “Experimental Results and Computational Fluid Dynamics Simulations of Labyrinth and Pocket Damper Seals for Wet Gas Compression,” ASME J Gas Turb Pwr, **138**, p. 052501.

[8] Beatty, P. A., and Hughes, W. F., 1987, "Turbulent Two-Phase Flow in Annular Seals," ASLE Trans., **30**(1) pp. 11-18.

[9] Beatty, P. A., and Hughes, W. F., 1990, "Stratified Two-Phase Flow in Annular Seals," ASME J. Tribol., **112**(2) pp. 372-381.

[10] San Andrés, L., 2012, “Rotordynamic Force Coefficients of Bubbly Mixture Annular Pressure Seals,” ASME J Gas Turb Pwr, **134**(2), p. 022503.

[11] Brennen, C. E., 2005, Fundamentals of Multiphase Flow, Cambridge University Press, NY, USA, Chap. 4, pp.132.

[12] Fritzen, C. P., 1986, "Identification of Mass, Damping and Stiffness Matrices of Mechanical System," ASME J. Vib. Acoust., **108**(1), pp. 9-16.

[13] San Andrés, L., 2012, "Experimental Identification of Bearing Force Coefficients," Modern Lubrication Theory, Notes 14, Texas A&M University Digital Libraries, College Station, TX.

[14] San Andrés, L., 2010, Modern Lubrication Theory, "Annular Pressure (Damper) Seals," Notes 12 (a), Texas A&M University Digital Libraries, http://oaktrust.library.tamu.edu/handle/1969.1/93252.

[15] Lu N.Q., Prosperetti, A., et al., 1990, "Underwater Noise Emissions from Bubble Clouds," IEEE J. Ocean. Eng., **15**(4), pp.275-281.

[16] Boley, B. A., Weiner, J. H., 1960, "Theory of thermal stresses," New York: Wiley 1960, pp. 288-291.

APPENDIX A. THERMAL EXPANSION OF THE SEAL CARTRIDGE

The seal clearance changes with the oil temperature, and is determined by the thermal expansion coefficient of the steel rotor (α_{steel}) and the acrylic seal cartridge ($\alpha_{acrylic}$). Appendix A shows the measured and predicted seal clearance for increasing of operating temperature.

The analysis follow the procedure in Ref. [16] and assumes both ends of the cylindrical seal cartridge are free (no constraint) and deform uniformly. The seal cartridge has an inner diameter (ID) r_a, and an outer diameter (OD) r_b shown in Figure 19. The ID and OD may have different temperatures T_a and T_b. The temperature distribution in this hollow cylinder is

$$T(r) = \left(\frac{T_b - T_a}{r_b - r_a}\right) \bullet \left(r - \frac{r_a + r_b}{2}\right) + \frac{T_b - T_a}{2} \tag{10}$$

where $T(r)$ is the radial temperature distribution, $T_a = T_{id} - T_o$ is the ID temperature rise, $T_b = T_{od} - T_0$ is the OD temperature rise, r_a is the ID radius, r_b is the OD radius, T_0 is a reference temperature.

The cylinder deformation $u(r)$ (assuming both ends unconstrained) due to temperature difference is [16]

$$u(r) = \frac{\alpha}{r(1-\nu)} \bullet \left[(1+\nu) \bullet \int_a^r T(r) r dr + \left[\frac{(1-3\nu) r^2 + a^2 (1+\nu)}{b^2 - a^2} \right] \int_a^b T(r) r dr \right] \tag{11}$$

where α is the material thermal expansion coefficient ($\alpha_{acrylic} = 75\times10^{-6}$ for acrylic material), ν is Possion's ratio (ν = 0.35 for acrylic material).

The seal assembled clearance is

$$C = C_{18^0 C} + (\mathrm{u}_{rotor}(\mathrm{r_a}) - \mathrm{u}(\mathrm{r_a})) \tag{12}$$

where $C_{18°C}$ = 0.127 mm is the measured seal assembled clearance at 18 ◦C, $u_{rotor}(r_a) = \alpha_{steel} \times T_a \times r_a$ is the rotor thermal expansion magnitude, where $\alpha_{steel} = 12\times10^{-6}$.

The calculation assumes the rotor OD temperature is identical to the seal cartridge ID temperature. Figure 20 presents the measured and calculated seal assembled clearance. The measurements are conducted immediately after each test without shaft speed. The predicted clearance is smaller than the measured results, but within uncertainty. The analysis shows

a simple hollow cylinder with both ends free is adequate to predict the *wet* seal assembled clearance.

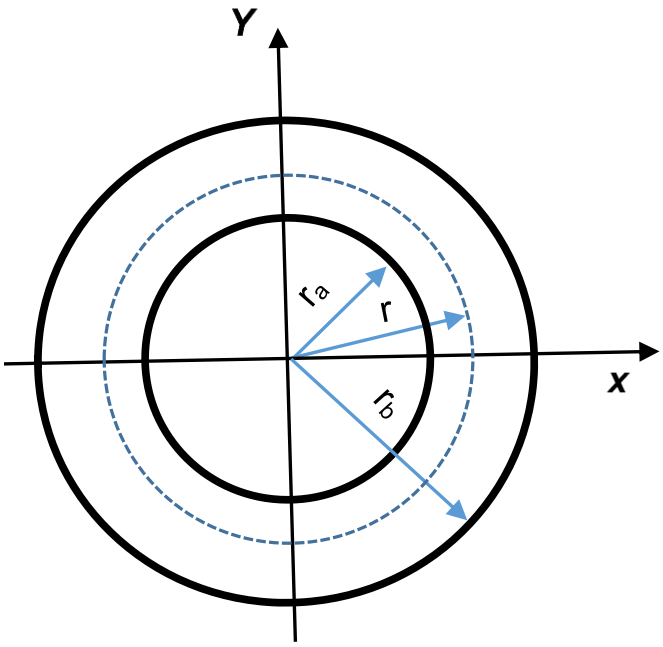

Figure 19. Top view of a hollow cylinder with ID = r_a, OD = r_b

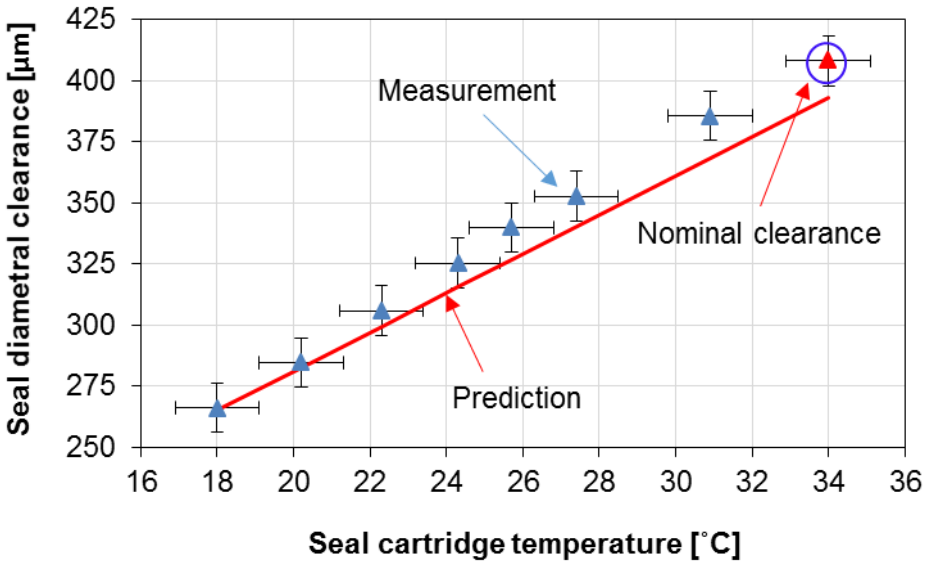

Figure 20. Seal diametral clearance vs. seal cartridge temperature, $C_{norminal}$ = 0.203 mm at 34 ºC, measured without shaft rotation.

APPENDIX B: IMAGINARY PART Im(H) AND DIRECT DAMPING (C) OF THE SEAL AT 2,500 RPM.

Appendix B shows the imaginary part of the seal complex stiffness Im(H_{ii}) when the seal operates with an air-oil mixture (GVF = 0 to 0.9), the shaft spinning speed is 2,500 rpm, and the supply pressure is 2.5 bar (abs)

Figure 21 shows the imaginary part of the seal complex stiffness Im(H_{XX}) and Im(H_{YY}). Graph (a) is Im(H_{XX}) and graph (b) is Im(H_{YY}). The symbols are test data, the lines are curve fit of the imaginary part Im(H_{XX}) $\leftarrow \omega_r C_{XX}$, and Im(H_{YY}) $\leftarrow \omega_r C_{YY}$.

Similar as the test result for operation with a shaft speed of 3,500 rpm, the seal imaginary part Im(H) increases proportionally with excitation frequency (ω) at an inlet GVF = 0 (pure oil). With gas content, imaginary part Im(H) is no longer proportional to frequency (ω), and cannot be characterized by a constant viscous damping (C). At a fixed excitation, i.e., 70 Hz, an increase in inlet GVF decrease significantly the imaginary stiffness Im(H_{XX}) and Im(H_{YY}).

Figure 22 shows the seal direct damping C_{XX} = Im(H_{XX}) / ω_r and C_{YY} = Im(H_{YY}) / ω_r at 2,500 rpm. The injection of air in to the oil strongly drops the seal direct damping, i.e., C_{XX} decreases form 22 kN.s/m at α_{inlet} = 0 to 6 kN.s/m at α_{inlet} = 0.9. The damping drops with frequency at inlet GVF up to 0.8. At an inlet GVF > 0.8, an increase in frequency does not affect much the seal direct damping (C).

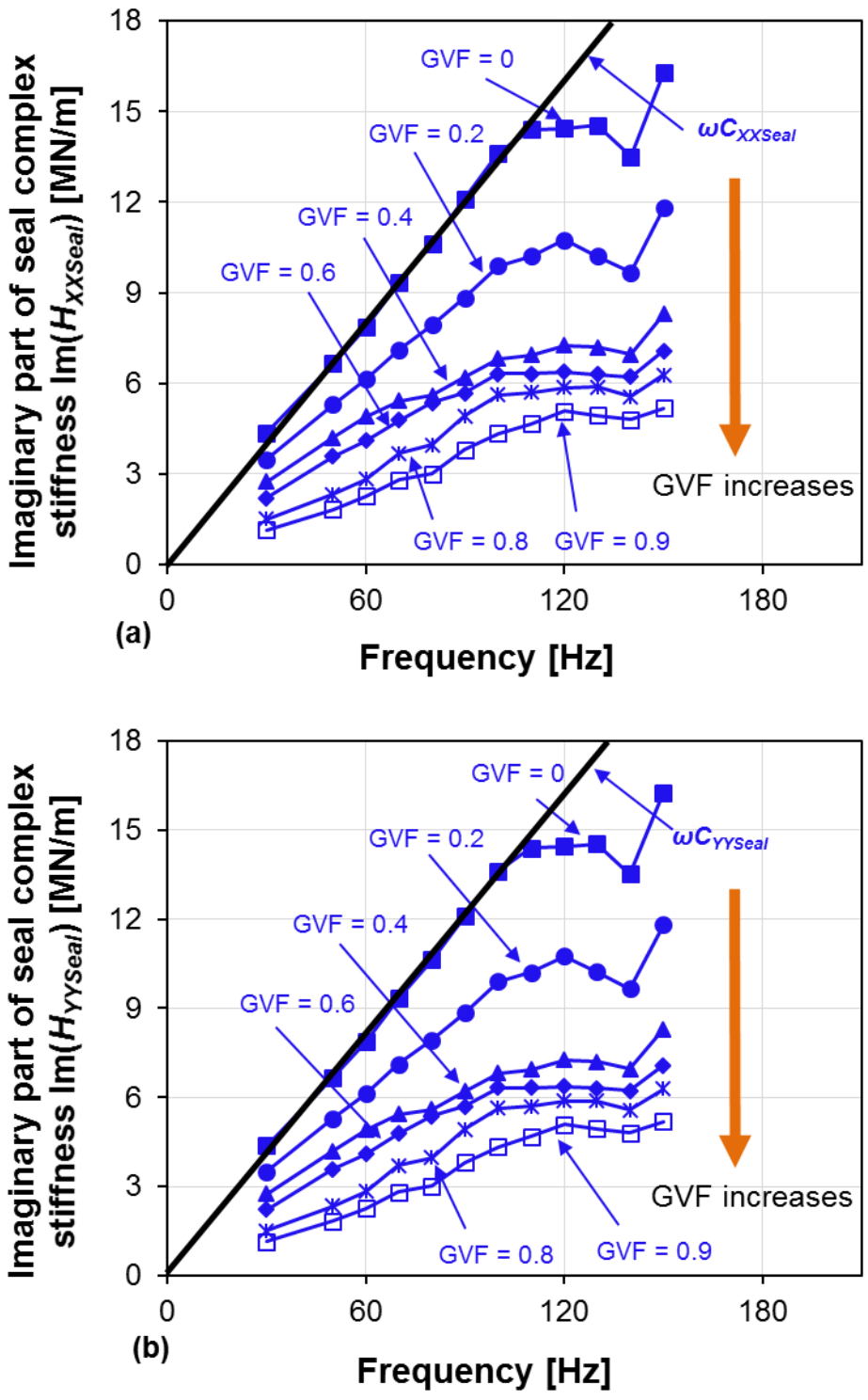

Figure 21. Imaginary part of seal complex stiffness Im(H_{XX}) and Im(H_{YY}) vs. whirl frequency (ω). Inlet GVF varies from 0 to 0.9. Shaft speed (N) = 2,500 rpm. Supply pressure (P_s) = 2.5 bar (abs), discharge pressure (P_a) = 1 bar (abs), oil temperature (T_{in}) = 33 ºC ~35 ºC.

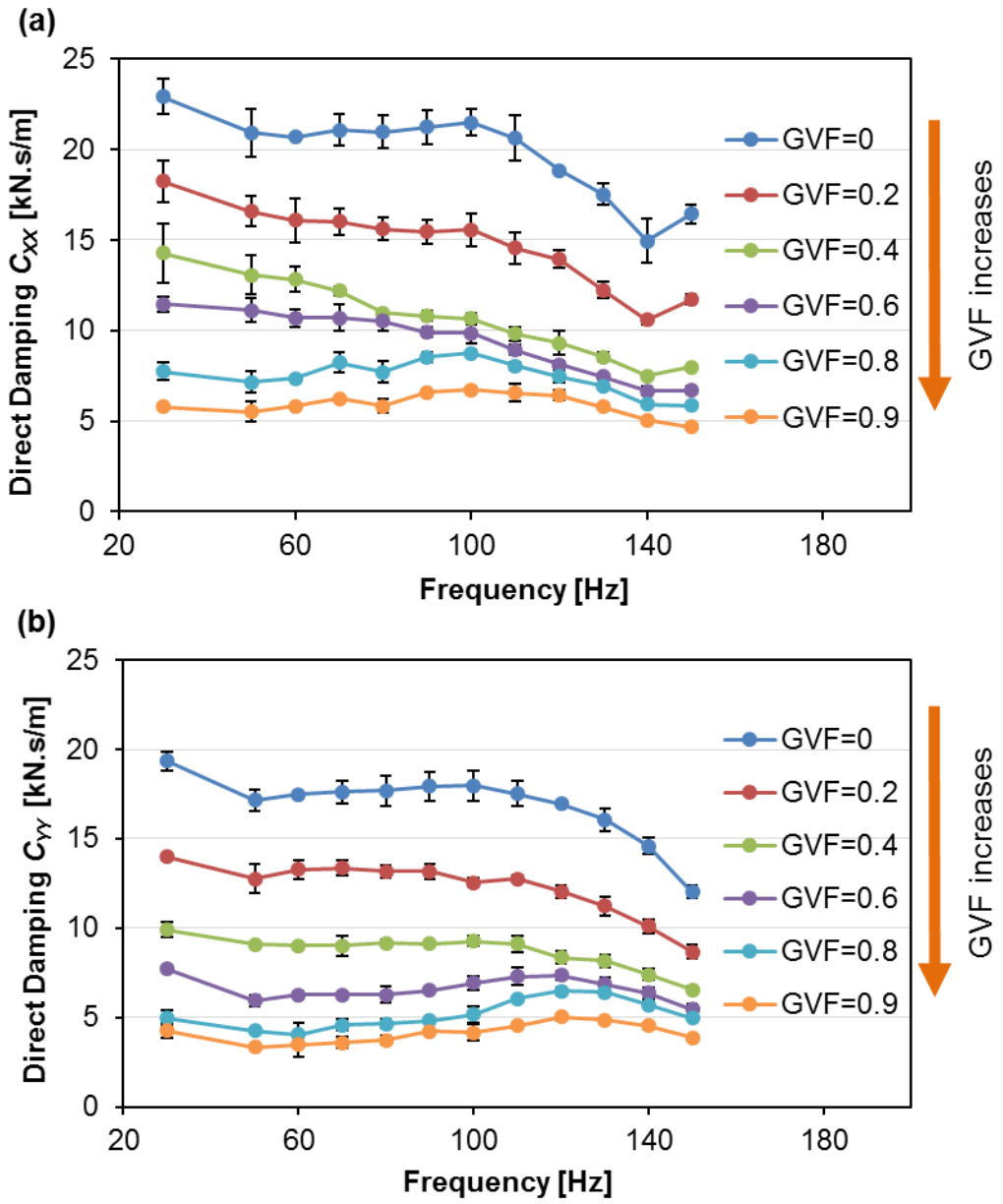

Figure 22. Experimental seal direct damping coefficient (C_{XX} and C_{YY}) vs. whirl frequency (ω). Inlet GVF varies from 0 to 0.9. Supply pressure (P_s) = 2.5 bar (abs), discharge pressure (P_a) = 1 bar (abs), inlet temperature (T_{in}) = 33 ºC ~35 ºC. Journal speed (N) = 2500 rpm.

APPENDIX C. SHEAR DRAG POWER IN SEAL

The seal drag power loss can be determined from measurements of power in the DC motor, i.e.

$$P_{seal} = P - P_{electric} - P_{mech} \tag{13}$$

where $P = VI$ is the test system total power consumption, V is the motor input voltage, and I is the current through the DC motor. $P_{electric} = I^2R$ is the electric power loss when the current I goes through the armature resistance $R = 0.06 \pm 0.01\ \Omega$ measured by a multimeter. P_{mech} is the power loss that consists of the motor bearings friction drag power, the loss from the transmission belt, and the windage from air drag, etc.

Assuming a homogeneous flow, the predicted seal drag power is

$$P_{seal} = 2\pi\Omega^2 R^3 \int_0^L \frac{1}{c}\mu_m dz \tag{14}$$

For operation at 1,500, 2,500 and 3,500rpm, Figure 23 shows the measured and predicted seal drag power vs inlet GVF. Test result show a steady drop of seal drag power as inlet GVF increases. An increase of mixture gas volume fraction drops its viscosity (μ_m), and hence reduces the seal drag power loss.

Prediction agrees well with test data at inlet GVF < 0.8. At $\alpha_{inlet} > 0.8$, the predicted drag power loss is only half of the measured data in magnitude. A possible reason is that at higher gas volume fractions, the mixture become inhomogeneous in the seal. The mixture viscosity (μ_m) during measurements is higher than the one used in the prediction.

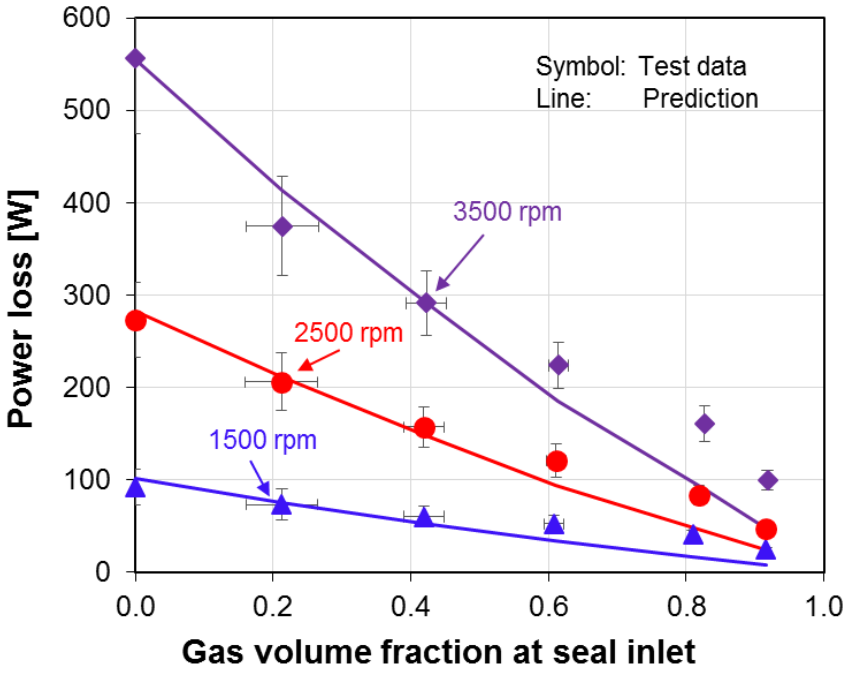

Figure 23. Seal drag power vs. inlet GVF. Shaft speed (*N*) = 1,500, 2,500, 3,500 rpm. Supply pressure (P_s) = 2.5 bar (abs), discharge pressure (P_a) = 1 bar (abs), oil temperature (T_{in}) = 33 ºC ~35 ºC.